

Evaluation and Application of Multi-decadal Visibility Data for Trend Analysis of Atmospheric Haze

C. Li¹, R. V. Martin^{1,2}, B. L. Boys¹, A. van Donkelaar¹, and S. Ruzzante^{1,3}

[1]{Department of Physics and Atmospheric Science, Dalhousie University, Halifax, NS, Canada}

[2]{Harvard-Smithsonian Center for Astrophysics, Cambridge, MA, USA}

[3]{Now at Department of Physics, Engineering Physics and Astronomy, Queen's University, Kingston, ON, Canada}

Correspondence to: C. Li (chi.li@dal.ca)

Abstract

There are few multi-decadal observations of atmospheric aerosols worldwide. This study applies global hourly visibility (Vis) observations at more than 3000 stations to investigate historical trends in atmospheric haze over 1945-1996 for the US, and over 1973-2013 for Europe and Eastern Asia. A comprehensive data screening and processing framework is developed and applied to minimize uncertainties and construct monthly statistics of inverse visibility ($1/\text{Vis}$). This data processing includes removal of relatively clean cases with high uncertainty, and change point detection to identify and separate methodological discontinuities such as the introduction of instrumentation. Although the relation between $1/\text{Vis}$ and atmospheric extinction coefficient (b_{ext}) varies across different stations, spatially coherent trends of the screened $1/\text{Vis}$ data exhibit consistency with the temporal evolution of collocated aerosol measurements, including the b_{ext} trend of $-2.4\% \text{ yr}^{-1}$ (95% CI: $-3.7, -1.1\% \text{ yr}^{-1}$) versus $1/\text{Vis}$ trend of $-1.6\% \text{ yr}^{-1}$ (95% CI: $-2.4, -0.8\% \text{ yr}^{-1}$) over the US for 1989-1996, and the fine aerosol mass ($\text{PM}_{2.5}$) trend of $-5.8\% \text{ yr}^{-1}$ (95% CI: $-7.8, -4.2\% \text{ yr}^{-1}$) versus $1/\text{Vis}$ trend of $-3.4\% \text{ yr}^{-1}$ (95% CI: $-4.4, -2.4\% \text{ yr}^{-1}$) over Europe for 2006-2013. Regional $1/\text{Vis}$ and Emissions Database for Global Atmospheric Research (EDGAR) sulfur dioxide (SO_2) emissions are significantly correlated over the eastern US for 1970-1995 ($r = 0.73$), over Europe for 1973-2008 ($r \sim 0.9$) and over China for 1973-2008 ($r \sim 0.9$). Consistent “reversal

1 points” from increasing to decreasing in SO₂ emission data are also captured by the regional
2 1/Vis time series (e.g. late 70s for the eastern US, early 1980s for Western Europe, late 1980s
3 for Eastern Europe, and mid 2000s for China). The consistency of 1/Vis trends with other in
4 situ measurements and emission data demonstrates promise in applying these quality assured
5 1/Vis data for historical air quality studies.

6

7 **1 Introduction**

8 Atmospheric aerosols have broad implications for air quality and climate change. The Global
9 Burden of Disease (GBD) assessment attributed ambient exposure to aerosol particles with an
10 aerodynamic diameter below 2.5 μm (PM_{2.5}) as the sixth largest overall risk factor for
11 premature mortality with 3.2 million premature deaths per year (Lim et al., 2012). Aerosols
12 are also considered as the most uncertain component for global radiative forcing (IPCC,
13 2013). Aerosols are formed from a variety of emission sources and chemical processes with a
14 short tropospheric lifetime against different removal mechanisms, yielding a highly variable
15 spatiotemporal distribution that is not well understood (Fuzzi et al., 2015). Information on
16 long-term aerosol temporal evolution is crucially needed across a range of disciplines.
17 Historical PM_{2.5} exposure and its trends are needed to understand changes in Global Burden
18 of Disease (Brauer et al., 2012), and to guide mitigation actions (Apte et al., 2015; Wong et
19 al., 2004). Observations are needed to evaluate historical emission inventories that are crucial
20 to accurately represent the changes in aerosol sources and its consequent feedbacks on climate
21 (Lu et al., 2011; S. Smith et al., 2011a; Xu et al., 2013). Aerosol trend analysis is also
22 fundamental to assessing radiative forcing, evaluating model processes, and projecting future
23 changes (Chin et al., 2014; Leibensperger et al., 2012; Li et al., 2014). Various studies have
24 been carried out to investigate aerosol trends using in situ measurements (Collaud Coen et al.,
25 2013; Hand et al., 2012a; Murphy et al., 2011), satellite/ground remote sensing (Hsu et al.,
26 2012; Li et al., 2014; Zhang and Reid, 2010), and analysis of measurements with models
27 (Boys et al., 2014; Chin et al., 2014; Pozzer et al., 2015; Turnock et al., 2015). However these
28 studies are mostly limited to the recent 2 decades, since few satellite or in situ aerosol
29 observations exist over land prior to the 1990s. Long-term observations of aerosols at the
30 global scale are needed to place current knowledge of their spatial distribution and temporal
31 evolution in a historical context for all these applications.

1 Visibility observations offer an alternative information source to investigate historical aerosol
2 trends. Horizontal visibility (Vis) from worldwide meteorological stations and airports is
3 mainly determined by the optical extinction (b_{ext}) of the atmospheric boundary layer, and has
4 been recognized as a proxy of the atmospheric aerosol burden/loading (Husar et al., 2000).
5 Historical Vis data from more than 3000 stations have been applied to characterize decadal
6 trends in global aerosol optical depth (AOD) from 1973 to 2007 (Wang et al., 2009). Regional
7 trend studies of Vis were also conducted for populated areas e.g. the US (Husar et al., 1981;
8 Schichtel et al., 2001), Europe (Vautard et al., 2009) and China (Che et al., 2007; Chen and
9 Wang, 2015; Lin et al., 2014; Wu et al., 2012; Wu et al., 2014), and the inferred trends were
10 usually attributed to changes in anthropogenic emission. Another study employing Vis over
11 desert regions (Mahowald et al., 2007) found an association of Vis with meteorology factors
12 such as drought index (based on precipitation and temperature) and surface wind speeds.
13 Trends in Vis data interpreted with other datasets also supported studies of several aerosol
14 related climate trends such as the western Pacific subtropical high (Qu et al., 2013) and
15 precipitation (Rosenfeld et al., 2007; Stjern et al., 2011).

16 Despite the abundance of the above mentioned studies, the interpretation of Vis data and its
17 trends might be limited by insufficient data processing or poor data quality. Multi-decadal Vis
18 data might contain possible variation or even reversal in haze trends as expected from
19 historical emission and surface solar radiation (SSR) data (Lu et al., 2010; Stern, 2006; Streets
20 et al., 2006; Wild et al., 2005). It is of particular interest how these changes would associate
21 with the trends of air quality, and would be captured by the Vis data. Detailed variation in
22 global Vis trends are rarely reported in these previous studies. On the other hand, Vis data are
23 inherently uncertain because most Vis are recorded through human observations with variable
24 protocols. For example, an increase in inverse visibility ($1/Vis$) has been reported over the US
25 during 1993-2010 (Wang et al., 2012) that is opposite in sign with the significant decline
26 ($>10\%$ decade⁻¹) of observed PM_{2.5}, sulfate and b_{ext} (Attwood et al., 2014; Hand et al., 2012a;
27 Hand et al., 2014; US EPA, 2012), and raises questions about the quality of Vis observations.

28 This study revisits the Vis observations to characterize historical trends of atmospheric haze
29 by asserting two major efforts: a more comprehensive data quality assurance processing and a
30 more detailed trend analysis for separate periods. This analysis provides multi-decadal
31 information about air quality evolution and its connections to emission trends over major
32 industrialized regions. To facilitate interpretation, the theoretical relationship between Vis and

1 atmospheric extinction is reviewed in the following section. Section 3 describes the data and
 2 processing methods, followed by an evaluation of the screened monthly $1/Vis$ and its trends
 3 using in situ measurements in Section 4. Section 5 provides an extensive discussion of the
 4 resultant spatial distribution and temporal variation of the derived $1/Vis$ trends for three
 5 highly populated regions (i.e. the US, Europe and Eastern Asia), and comparative analysis of
 6 these trends with sulfur dioxide (SO_2) emission data. The final section summarizes this work
 7 and its implications.

8

9 **2 Relationship between Vis and b_{ext}**

10 Visibility is a measure of the transparency of the atmosphere, and is defined as the greatest
 11 distance at which a black object can be recognized against the horizon sky (WMO, 2008). The
 12 visibility of a particular object (i.e. visibility marker) is determined by the contrast C between
 13 the radiation intensity I of the background b and of the object o reaching an observer at
 14 distance x from the object:

$$15 \quad C(x) = \frac{I_b(x) - I_o(x)}{I_b(x)} \quad (1)$$

16 Under assumptions of a plane-parallel atmosphere and homogeneous background intensity
 17 (i.e. constant sky brightness), C exhibits an exponential decay based on Beer's law,

$$18 \quad C(x) = C_0 \exp(-b_{ext}x) \quad (2)$$

19 where b_{ext} is the extinction of the atmosphere (including extinction of aerosols and
 20 molecules). Since Vis represents the furthest distance corresponding to a minimum critical
 21 contrast C_{crit} below which the observer cannot discern the object, we have

$$22 \quad C_{crit} = C_0 \exp(-b_{ext}Vis) \quad (3)$$

23 Rearranging to solve for b_{ext} yields

$$24 \quad b_{ext} = \frac{K}{Vis} \quad (4)$$

25 where $K = -\ln \frac{C_{crit}}{C_0}$. This is the Koschmieder equation (Griffing, 1980), representing a linear

26 relationship between $1/Vis$ and b_{ext} . The slope K of this relationship is mainly determined by
 27 two factors: the inherent contrast at the object's position C_0 and the critical contrast of the

1 observer's eye C_{crit} . This equation is only valid for a plane-parallel and homogeneous
2 atmosphere. For situations with high gradients of b_{ext} (e.g. smoke plumes), this could readily
3 break down. Even for ideal conditions, this relationship could vary due to the variation of C_0
4 (change of markers or observing conditions) and/or C_{crit} (change of observer or protocol). It is
5 sometimes assumed that the object is perfectly black ($C_0 = 1$) so that K is only determined by
6 C_{crit} . Nevertheless, K still varies from 1.5 to 3.9 (e.g. Husar and Wilson, 1993; Schichtel et al.,
7 2001; Wang et al., 2009) because of different C_{crit} values or different observing conditions.
8 Below we similarly find that even where $1/Vis$ is highly correlated with b_{ext} data, K still varies
9 significantly for different stations.

10

11 **3 Data and processing**

12 **3.1 Visibility data**

13 We begin with raw Vis data from synoptic observations over 1929-2013 in the Integrated
14 Surface Database (ISD, <https://catalog.data.gov/dataset/integrated-surface-global-hourly-data>)
15 archived at the NOAA's National Centers for Environmental Information (NCEI). ISD data
16 are generated through merging hundreds of data sources (A. Smith et al., 2011). The data
17 from different networks have different report frequencies (e.g. hourly, 3-hourly, 6-hourly,
18 etc.). We reject the daily averaged data called "global summary of the day" (GSOD) since an
19 arithmetic mean could bias the daily and monthly statistics because of threshold and
20 discreteness issues, as discussed in Section 3.1.2. Each processing step is described below.

21 **3.1.1 Conventional screening**

22 We begin with "conventional screening" using algorithms adapted from prior studies. We
23 eliminate effects on Vis of weather conditions such as fog, precipitation, low cloud and high
24 relative humidity ($RH > 90\%$, estimated from temperature and dew point) following the
25 description in Husar et al. (2000). A sensitivity test that limited conditions to $RH < 80\%$
26 reduced data density but yielded similar trend results without changing the main findings in
27 this study. Potential human errors are reduced by statistical checks of daily spikes and non-
28 repeating values following Lin et al. (2014). Duplicate stations with different names are
29 combined, and stations lacking geolocation information are removed following Willett et al.
30 (2013). After this screening step, 21,703 stations remain from the 30,895 original ISD sites.

1 **3.1.2 Threshold filtering**

2 We develop a filter to address spatial and temporal variation in the threshold of reported Vis.
3 The “threshold” is the maximum reported Vis at a station that often depends on the furthest
4 employed Vis marker. Vis above this threshold is not resolved. Thus the threshold acts as an
5 artificial detection limit. The ability of Vis data to capture the variation of b_{ext} is weak when
6 the air is clean and/or the adopted threshold Vis at the station is low. We identify the 99th
7 percentile of reported Vis in each year as the threshold for each station, and reject months
8 with $\leq 50\%$ of the data below the threshold. This approach differs from eliminating stations
9 with low thresholds (e.g. Husar et al., 2000). Observations could still be meaningful at heavily
10 polluted stations even if the threshold is low, while for clean stations with high thresholds
11 most of the reported Vis could remain unresolved. To further ensure data representativeness
12 and variability, data are removed for any month with less than 4 different days of data or with
13 nearly identical percentile values (i.e. the ratio of 50th and 25th percentile Vis is less than
14 1.07 or the ratio of the 25th to 10th percentile Vis is less than 1.1) following Husar et al.
15 (2000). This data screening step further reduces the number of qualified station to 10,446.

16 We describe the monthly Vis level with nonparametric statistics rather than arithmetic mean
17 for a few reasons. First, an arithmetic mean would have biased monthly statistics due to the
18 variable fraction (50-100% after the threshold filtering) of Vis reported under the threshold in
19 one month. Second, Vis is recorded as discrete values with coarse and uneven increments, and
20 is not normally distributed (Schichtel et al., 2001). The protocol of reporting Vis varies across
21 stations, depending on local regulations and available Vis markers. Both issues would affect
22 the GSOD data or the monthly mean $1/\text{Vis}$ so we work with the raw data. We follow the
23 convention to adopt the 75th percentile $1/\text{Vis}$ as the monthly representation of haziness
24 (Husar et al., 2000; Qu et al., 2013). Other statistics, such as 50th and 90th percentile $1/\text{Vis}$
25 lead to similar trends and do not alter the conclusion of this study. However, the 50th
26 percentile is closer to and more vulnerable to the detection limit, while the 90th percentile
27 tends to be more susceptible to extreme events. Husar and Patterson (1987) assessed the
28 effects of different choices of statistics. Below we commonly refer to the 75th percentile as
29 “monthly $1/\text{Vis}$ ” unless stated otherwise.

1 **3.1.3 Completeness check**

2 Completeness criteria are applied for further screening. A year of data is removed if less than
3 6 months in this year is available to guarantee annual representativeness. Short-term time
4 series covering less than 7 years are also removed since they offer little information on trends.
5 A total of 6,466 stations comply with these standards and remain in the data archive.

6 **3.1.4 Change point detection**

7 Sudden discontinuities in characteristics of the derived monthly time series of $1/Vis$ are
8 frequently found even after the comprehensive filtering. Any change of the Vis marker (i.e.
9 change of C_0) or observing standard (i.e. change of C_{crit}) could alter the relationship (K)
10 between b_{ext} and $1/Vis$, introducing inconsistency in the time series unrelated to actual b_{ext}
11 change. For example, instrumentation (e.g. telephotometers, transmissometers and
12 scatterometers) has replaced human observers at many sites in the US (Kessner et al., 2013)
13 and to a lesser extent in Europe (Vautard et al., 2009), but there is a lack of documentation
14 recording when and at which stations this switch occurred. Such artificial changes could
15 seriously bias the inferred trends if not addressed. Various methods have been proposed to
16 detect abrupt “change points” (Costa and Soares, 2009; Reeves et al., 2007). For example, the
17 RHtest software package developed for multiple change point detection is based on penalized
18 maximal t and F test (Wang, 2008a; Wang et al., 2007) embedded in a recursive testing
19 algorithm (Wang, 2008b). We adopt the FindU function in the RHtest (version 4, available at
20 <http://etccdi.pacificclimate.org/>) software to detect “type-1” change points (without reference
21 time series). We manually examine all reported change points for possible false detections.
22 By visually inspecting each remaining station from Section 3.1.3, we retain only obvious
23 structural discontinuities in the time series of 50th or 75th monthly percentiles from the
24 candidate change points provided by the RHtest results.

25 Figure 1 shows an example of change point detection based on the time series of 50th and
26 75th percentiles of monthly $1/Vis$ at one ISD station. The change points are reported in 3
27 different types (95% confidence): significant change, possibly significant (undetermined)
28 change and insignificant change. In this example, although 4 significant changes for the 50th
29 percentiles $1/Vis$ and 2 significant change points for the 75th percentiles $1/Vis$ are reported,
30 only one candidate (February, 1988) indicated by both time series is considered as an obvious
31 discontinuity and chosen as the actual change point.

1 The candidate change points provided by RHtest allow greater efficiency than pure manual
2 detection, which is prohibitive for thousands of stations. Any gap of more than 4 years in a
3 time series is also considered as a change point. Such a large gap could obscure protocol
4 changes and introduce uncertainties in the derived trends without separation. We analyze
5 separately the 1/Vis time series before and after the determined change points. Finally, we
6 eliminate any year of data with annual 1/Vis (average of monthly 1/Vis) less than 40 Mm^{-1} to
7 address the poor data variation and representativeness of clean environments, as will be
8 discussed in Section 4.1.

9 We acknowledge that, although guided by RHtest results and a synthetic analysis based on the
10 time series of 50th and 75th percentiles, this is still a subjective method. A small fraction of
11 determined change points could be extreme events, while a few undetected change points
12 missed by this subjective judgement might remain in the analysis. Several time series with
13 irregular temporal variation are also removed during the visual examination. In summary,
14 only 1/Vis time series considered as consistent and continuous are analyzed here.

15 A total of 3,930 stations (5,320 time series) remain after this processing step, in which 856
16 sites (22%) are diagnosed as containing change points and thus separated. This small fraction
17 of structural discontinuities generally has minor impacts on the large-scale trend features and
18 regional trends in Section 5 according to our sensitivity test using data without separation. But
19 the separated data reduce spatial incoherency in the derived trend maps, and are more reliable
20 for studies over small areas or independent stations, as shown in Fig. 1.

21 The threshold filtering (Section 3.1.2) and change point detection (Section 3.1.4) are designed
22 to ensure basic representativeness and continuity of the derived monthly 1/Vis time series,
23 and are the main differences of this processing from prior investigations.

24 **3.1.5 Distribution of stations**

25 Figure 2 (top) shows the ISD stations and the number of years with available data for 1929-
26 2013 before and after data processing. Most of the remaining stations are located in the US
27 (753), Europe (1625) and Eastern Asia (791). More than 6000 removed stations have less than
28 7 years of data as indicated in the left panel. Many other removed stations have small
29 population density or harsh observing environment (e.g. islands and polar regions), which
30 might correspond to poor observing conditions or maintenance.

1 Figure 2 (bottom) shows that most US stations are screened after the mid 1990s. This is
2 because more than 90% of the ISD stations gradually switched to employ a low Vis threshold
3 of 10 miles (~16 km) after the mid 1990s (Fig. A1), probably due to the introduction of
4 unified instrumentation (Kessner et al., 2013). A maximum Vis of 16 km may be sufficient
5 for airport navigation and weather reports, but this threshold Vis under clear sky conditions
6 represents a moderate pollution level, and clean cases are not resolved. Thus most of the US
7 stations with such low thresholds are rejected during the threshold screening. In contrast,
8 screened stations remain densely distributed with long-term data over Europe and Eastern
9 Asia after the mid 1990s because the adopted thresholds are generally higher and more
10 consistent (Fig. A1).

11 **3.2 Complimentary in situ data**

12 We adopt complimentary data to evaluate and interpret the constructed monthly $1/\text{Vis}$ time
13 series and trends. The measured and calculated aerosol optical data from the Interagency
14 Monitoring of PROtected Visual Environments (IMPROVE) programme
15 (<http://vista.cira.colostate.edu/improve/Data/data.htm>) are employed to evaluate the screened
16 $1/\text{Vis}$ data and its trends after 1988. IMPROVE applies empirical mass extinction and RH
17 growth factors to measured mass of aerosol components to calculate and report ambient b_{ext} in
18 a 3-4 day frequency (Pitchford et al., 2007), and for several stations concurrent measurements
19 of aerosol scattering coefficient (b_{sp}) are also made at hourly frequency using nephelometers.
20 We generate monthly mean total b_{ext} (including aerosol extinction and site-specific Rayleigh
21 scattering) and b_{sp} from data with RH < 90% and status flags as “V0” (valid). Any month with
22 less than 4 available days for averaging is abandoned. Pitchford et al. (2007) demonstrated
23 that the estimated b_{ext} is consistent with measured b_{sp} . We also find high correlation ($r = 0.90$,
24 $N = 3439$) between monthly b_{ext} and b_{sp} across IMPROVE stations (Fig. A2).

25 The measurement of b_{ext} or b_{sp} is sparse outside the US. Therefore we obtain long-term
26 measurements of fine particulate matter mass ($\text{PM}_{2.5}$) from the European Monitoring and
27 Evaluation Programme (EMEP, <http://ebas.nilu.no>) for comparison over Europe (Tørseth et
28 al., 2012). Forty-five stations of data collected by filter-based ambient samplers are used.
29 Similarly, these daily $\text{PM}_{2.5}$ data are averaged monthly provided at least 4 valid measurements
30 are available.

1 **3.3 SO₂ emission data**

2 We apply bottom-up total anthropogenic SO₂ emission inventories to interpret historical 1/Vis
3 trends. This approach exploits the close relation of sulfate aerosol concentration with SO₂
4 emission due to the short time scale of SO₂ oxidation (Chin et al., 1996; Chin et al., 2014;
5 Daum et al., 1984; Hand et al., 2012a), the major PM_{2.5} contribution from sulfate aerosols
6 over land for most populated areas (Chin et al., 2014; Philip et al., 2014), and the dominance
7 of sulfate for light extinction due to its hygroscopicity (Hand et al., 2014). We employ 3
8 different SO₂ emission datasets, including country-level data for 1850-2005 (S. Smith et al.,
9 2011 a, b), gridded data from EDGAR (Emissions Database for Global Atmospheric
10 Research) version 4.2 (EC-JRC/PBL, 2011) at 0.1 degree resolution for 1970-2008
11 (<http://edgar.jrc.ec.europa.eu/>), and data from Lu et al. (2011) at 0.5 degree resolution for
12 1996-2010 over China. The data from S. Smith et al. (2011a) are referred to as “Smith
13 emissions” below. The data from Lu et al. (2011) are referred to as “Lu emissions”.

14 **3.4 Trend analysis**

15 In this study, we separately calculate trends for several periods of 8-10 years to allow possible
16 trend reversal, and to include stations with short-term data. The choice of study periods is
17 mainly based on the historical SO₂ emission data. Figure A3 shows the Smith emission data
18 for several representative countries. SO₂ emission trends in the US changed direction at
19 ~1944, ~1954, and again at ~1973. Also, for most Eastern European countries, there is a sharp
20 reduction of SO₂ emission starting from ~1989 after the breakdown of the communist system,
21 while the 1997 Asian financial crisis affected the SO₂ emission trend in Korea. It is of
22 particular interest to examine how Vis is affected by these emission changes. Data for most
23 ISD stations outside the US start from the year 1973, and representative coverage of Vis
24 stations over the US starts from the year 1945, although the earliest records after screening
25 start from 1929. Based on these transition points of SO₂ trends and Vis data availability, 8
26 periods (1945-1953, 1954-1963, 1964-1972, 1973-1980, 1981-1988, 1989-1996, 1997-2005,
27 2006-2013) are chosen to be analyzed in detail over the US, while the latter 5 periods are
28 studied for Europe and Eastern Asia. We also briefly examine two short periods before 1945
29 (1929-1934 and 1935-1944) over the US where stations are less spatially representative (not
30 included in regional quantitative analysis) but still show prominent trend information in 1/Vis.

1 We assess the linear trend and its significance (p value, two-tail test) in the deseasonalized
2 monthly anomalies using Sen's slope (Sen, 1968) and the Mann-Kendall (MK) test (Kendall,
3 1975; Mann, 1945). All monthly data are deseasonalized by removing multi-year monthly
4 means of each period before trend estimation. Pre-whitening is introduced to reduce the effect
5 of lag-1 autocorrelation (Yue et al., 2002), and 95% confidence interval (CI) of the slope is
6 calculated (Li et al., 2014). This nonparametric trend estimation method is insensitive to
7 missing values and outliers in the time series, and does not require a normal distribution, thus
8 it has been widely adopted to study aerosol trends in previous studies (Collaud Coen et al.,
9 2013; Papadimas et al., 2008). Least square trends (Weatherhead et al., 1998) are also
10 calculated, and are found to be consistent with the MK-Sen trends. For all the 8027 calculated
11 slopes in 1/Vis, 88% are unanimously diagnosed as significant (90% confidence, $p < 0.1$) or
12 insignificant by both methods. For the significant trends 76% of their differences are within
13 20%. Relative trends are calculated by normalizing the absolute MK-Sen slopes to the multi-
14 year mean of monthly 1/Vis in the corresponding period to facilitate the comparison and
15 interpretation with other in situ data.

16 Short-term trends of 8-10 years are expected to be less statistically robust and more sensitive
17 to extremes. For each period, a time series is required to contain at least half of the total
18 months and 2/3 of the total years (e.g. at least 60 monthly data in at least 7 years for a 10 year
19 period) for the calculated trend to be representative. This step only reduces the number of
20 stations at which trends are reported, but does not further screen the data.

21 The meaning and observing methods of daytime and nighttime data differ. According to
22 WMO (2008), Vis at night, as determined using illuminated objects, also depends on the light
23 source intensity, the adaptation of the observer's eyes to darkness and the observer's
24 illuminance threshold. We compare the relative trends calculated using daytime and nighttime
25 data to the combined trends adopted in this paper, over all remaining sites and the 8 periods.
26 The 5183 daytime trends have a correlation of 0.85 with the combined trends, in which 84%
27 of the differences between significant trends ($p < 0.1$) are within 50%. For the comparison
28 between 4109 nighttime and combined trends, the correlation is 0.80 and 78% of the
29 differences between significant trends are within 50%. Therefore, after representing the data
30 into a monthly resolution and normalizing the changes in 1/Vis into relative trends, the
31 daytime and nighttime data show generally consistent trends in haze level compared to the
32 combined data, and do not meaningfully alter our results and conclusions.

1 We calculate composite trends based on monthly $1/\text{Vis}$ averaged from an ensemble of stations
2 (e.g. for the time series of collocated stations in Section 4 or defined regions in Section 5). To
3 ensure temporal representativeness, a station is considered in the average only if 2/3 of the
4 total months of data are available for the study period. Qualified stations are gridded to 1
5 degree resolution before averaging to avoid biased averaging towards more densely
6 distributed areas. To ensure spatial representativeness, only monthly data derived from at least
7 75% of the total grids (i.e. number of unique grids covered by all the monthly data) for each
8 study period are used in the composite trend estimation. This strategy reduces sampling
9 difference within each periods, however the composite $1/\text{Vis}$ for different periods might be
10 averaged from a different distribution of stations. We expect the uncertainty from spatially
11 variant K and data quality to be random, and to be reduced by spatial averaging and by
12 normalizing the slopes into relative trends. Over these regions, we also calculate several time
13 series and trends for longer merged periods with consistent station coverage and similar
14 trends, to assess the consistency of the short-term trends.

15

16 **4 Evaluation against in situ data**

17 **4.1 Comparison with IMPROVE b_{ext} and EMEP $\text{PM}_{2.5}$**

18 We compare the monthly IMPROVE b_{ext} data with the quality controlled monthly $1/\text{Vis}$ from
19 Section 3.1. Collocations are considered between IMPROVE and ISD time series over 1988-
20 2013 within the distance of less than 1 degree and altitude difference of less than 500 m. One
21 IMPROVE station could pair with more than one ISD station and vice versa. Fifty-nine
22 collocations (each with at least 20 paired monthly values) are made. We expect a maximum
23 correlation of 0.9 given the relation between measured b_{sp} and calculated b_{ext} (Fig. A2).
24 Similarly, we create collocations between ISD $1/\text{Vis}$ and EMEP $\text{PM}_{2.5}$ on a monthly basis,
25 and expect a weaker correlation due to variation of aerosol water and mass extinction
26 efficiency.

27 Figure 3 shows the comparison results between collocated $1/\text{Vis}$ and b_{ext} over the US. This
28 evaluation highlights several major findings:

29 1) The mean b_{ext} level of collocated IMPROVE stations after 1990 is below 50 Mm^{-1} for the
30 western US, and below 120 Mm^{-1} for the eastern US (top left). As discussed in Section 3.1,
31 the low threshold Vis of $\sim 16 \text{ km}$ (equivalent to $b_{ext} \sim 100 - 240 \text{ Mm}^{-1}$ depending on K)

1 recently adopted by most US stations fails to resolve actual b_{ext} variation under this relatively
2 clean environment. Thus many stations are rejected by the threshold filtering.

3 2) As shown in the top right panel, correlation coefficients of monthly values vary from ~ 0 to
4 0.85. About half of the collocations (29 out of 59) have $r < 0.5$, while 10 collocated ISD
5 stations have $r > 0.7$. The overall moderate correlation is not unexpected, as is similarly found
6 in previous studies (Mahowald et al., 2007; Wang et al., 2012). Correlations are expected to
7 differ from station to station, due to the inherent difference in observing conditions, protocols,
8 and residual uncertainties. This preliminary evaluation suggests that Vis data at individual
9 stations can be unreliable, and in the following discussion we focus on interpreting regionally
10 coherent observations.

11 3) Correlations generally exceed 0.5 in the eastern US, where the mean b_{ext} is higher due to
12 higher aerosol concentration (Hand et al., 2012b; van Donkelaar et al., 2015) and to a larger
13 fraction of hygroscopic sulfate aerosols (Hand et al., 2012b). The correlation increases
14 significantly with the mean b_{ext} , indicating the tendency for better $1/Vis$ representativeness in
15 more polluted regions. As previously discussed, at lower b_{ext} more reported Vis are close to
16 the threshold Vis, thus the true $1/Vis$ tends to be less well resolved. Also, because the Vis data
17 are reported in discrete values, clean stations with a narrow dynamic range of b_{ext} have few
18 reportable Vis to capture the continuous b_{ext} variation. Moreover, the increment of adjacent
19 reportable Vis is relatively coarse in cleaner conditions (WMO, 2008), and atmospheric
20 homogeneity might break down for longer distances. All these factors weaken the ability of
21 Vis to capture b_{ext} variation in clean environments. Wang et al. (2012) found low correlation
22 of $1/Vis$ with PM_{10} over the US and Canada, and similarly attributed this to low aerosol
23 concentrations and higher Vis uncertainty over North America. Thus we apply the 40 Mm^{-1}
24 threshold of annual $1/Vis$ to further filter the data as introduced in Section 3.1.4. Without this
25 screening, 7 of 8 stations with mean $1/Vis < 40 \text{ Mm}^{-1}$ were found to exhibit low correlations
26 ($r < 0.25$) with collocated b_{ext} . Different thresholds from 10 to 70 Mm^{-1} were tested, and
27 thresholds above 40 Mm^{-1} ceased to improve the consistency with the few sites reporting b_{ext} .

28 4) The slope of fitted linear relationship (bottom left) between $1/Vis$ and b_{ext} varies from ~ 0.8
29 to ~ 2 even over the eastern US where correlations are higher. This supports the expectation
30 that this slope (K) would differ spatially with observing conditions (Griffing, 1980; Husar et
31 al., 2000; Schichtel et al., 2001), as discussed in Section 2. Thus in the later analysis we focus
32 on the relative trend of $1/Vis$ which is independent of K .

1 Figure 3 (bottom right) also shows the correlation between monthly $1/\text{Vis}$ and $\text{PM}_{2.5}$ over
2 Europe. Although the relation of $1/\text{Vis}$ with $\text{PM}_{2.5}$ is expected to be more uncertain than with
3 b_{ext} , we find more stations with high correlation ($r > 0.5$) over Europe (93 out of 129, 72%)
4 than over the US (51%). Wang et al. (2012) similarly found higher correlation of $1/\text{Vis}$ with
5 PM_{10} over Europe and China than over the US and Canada. The higher thresholds and higher
6 concentration of fine aerosol over Europe (van Donkelaar et al., 2015) allow $1/\text{Vis}$ to better
7 resolve $\text{PM}_{2.5}$ variation there. These findings suggest more reliability of Vis observations at
8 areas with both higher aerosol loading and sufficiently high thresholds to resolve b_{ext}
9 variation, e.g. the three populated regions investigated in this study.

10 **4.2 Trend evaluation**

11 Figure 4 shows the spatial distribution of relative trends in $1/\text{Vis}$, in IMPROVE estimated b_{ext}
12 and in measured b_{sp} over the US for 1989-2013. Overall, the trend maps of $1/\text{Vis}$, b_{ext} and b_{sp}
13 show a dominant trend of decreasing haziness over the continental US after 1988, which
14 reflects reduction of aerosol sources (Hand et al., 2014; Leibensperger et al., 2012). The
15 overall decrease across the US is consistent with recent trend studies employing IMPROVE
16 b_{ext} (Hand et al., 2014) and b_{sp} (Collaud Coen et al., 2013) data, and is determined by the
17 reduction of both aerosol mass and hygroscopicity (Attwood et al., 2014). For the last 2
18 periods (1997-2013), the number of available ISD stations for trend analysis is dramatically
19 reduced by their detection limit and improved air quality. Although the remaining sparse ISD
20 stations still show overall consistency in trends with nearby b_{ext} and b_{sp} , they cannot provide
21 spatially coherent and aggregated trend information. We thus suggest that the ISD Vis data
22 over the US are not appropriate for studying haze trends after the mid 1990s, and limit our
23 analysis to data before 1996 for this region. Over 1989-1996, the $1/\text{Vis}$ trends still reproduce
24 the b_{ext} trends, with decreasing tendencies in the eastern and western US. For this period, 15
25 ISD stations and 9 IMPROVE stations with significant trends are collocated and labeled. Thus
26 the apparent discrepancy in sign of trends in $1/\text{Vis}$ (Wang et al., 2012) with trends in other
27 aerosol measurements (Attwood et al., 2014; Hand et al., 2012a; Hand et al., 2014; US EPA,
28 2012) is resolved by more comprehensive data processing and screening.

29 Figure 5 shows the spatial distribution of relative trends in $1/\text{Vis}$ and $\text{PM}_{2.5}$ over Europe for
30 2006-2013. There is a tendency of greater reductions in $1/\text{Vis}$ over Western Europe than over
31 Eastern Europe as examined further in Section 5.2. The dominant decreasing trends of $\text{PM}_{2.5}$

1 is well captured by the 1/Vis trends, especially at the 19 ISD and 10 EMEP collocated sites
2 with significant trends, as discussed further below.

3 Figure 6 (top) shows the composite time series of the collocated 1/Vis and b_{ext} stations over
4 the US for 1989-1996. The seasonal variation of the averaged b_{ext} is well reproduced by that
5 of collocated 1/Vis, with a correlation of 0.77 between these two time series. Both composite
6 1/Vis and b_{ext} show a peak in summer months, due mostly to increased aerosol concentration
7 in warm months because of increased photochemical activity and biogenic emission (Chen et
8 al., 2012; Hand et al., 2012b). The trend of collocated 1/Vis ($-1.6\% \text{ yr}^{-1}$; 95% CI: $-2.4, -0.8\%$
9 yr^{-1}) is within the confidence intervals of the decrease of b_{ext} ($-2.4\% \text{ yr}^{-1}$; 95% CI: $-3.7, -1.1\%$
10 yr^{-1}). The slight underestimation may reflect the weak sensitivity of discrete 1/Vis data to the
11 continuous decrease of b_{ext} in clean environments due to the threshold and discreteness issues.

12 Figure 6 (bottom) shows composite time series of $\text{PM}_{2.5}$ and 1/Vis of these collocated 1/Vis
13 and $\text{PM}_{2.5}$ stations over Europe for 2006-2013. High correlation (0.80) between these two
14 time series indicates consistent seasonal variation. The winter maximum in the composite
15 1/Vis over Europe well represents the $\text{PM}_{2.5}$ seasonality at most collocated EMEP sites, which
16 could be attributable to near surface inversion and low surface winds (Yttri et al., 2012), to
17 greater nitrate aerosol formation (Aas et al., 2012; Yttri et al., 2012), and to higher
18 carbonaceous aerosol emission from residential wood combustion (Denier van der Gon et al.,
19 2015). The CI of the 1/Vis trend ($-3.4\% \text{ yr}^{-1}$, 95% CI: $-4.4, -2.4\% \text{ yr}^{-1}$) overlaps with that of
20 the $\text{PM}_{2.5}$ trend ($-5.8\% \text{ yr}^{-1}$, 95% CI: $-7.8, -4.2\% \text{ yr}^{-1}$), but underestimates the relative decrease
21 of $\text{PM}_{2.5}$. In addition to the weak sensitivity of discrete 1/Vis to resolve aerosol variation
22 under clean environment (the collocated EMEP stations are mostly in the cleaner Western
23 Europe), the inclusion of Rayleigh scattering in 1/Vis and the non-linear association between
24 ambient 1/Vis and dry $\text{PM}_{2.5}$ (fixed at 50% RH) also contribute to this bias.

25 In summary, 1/Vis exhibits spatially variant K (i.e. relationship with b_{ext}) and data quality that
26 suggests uncertainty in the information of one station especially at clean locations. However
27 the aggregated 1/Vis time series successfully capture the seasonal variation and trends of
28 collocated in situ data. The high correlation between composite time series and the overall
29 consistency of composite trends suggest that the interpretation value of 1/Vis data benefits
30 from averaging over multiple stations.

31

1 **5 Historical Trends of 1/Vis**

2 **5.1 United States**

3 Figure 7 presents the calculated relative trend of 1/Vis of all qualified stations over the US for
4 1945-1988 (Fig. 4 contains 1/Vis trends over 1989-2013). Figure 8 shows the regionally
5 averaged time series and trends of 1/Vis over the eastern US for 1945-1996, superimposed
6 with the evolution of SO₂ emission data. Historically, 1/Vis in the eastern US experienced a
7 pronounced decrease (-2.8% yr⁻¹, p < 0.001) after World War II until the mid 1950s, a
8 consistent upward trend afterwards (0.9–1.8% yr⁻¹, p < 0.001) during the following 2 periods
9 until the early 1970s, variable tendencies during 1973-1980, and a significant decreasing trend
10 (-1.1 to -2.0% yr⁻¹, p < 0.005) from the early 1980s until 1996. Over 1954-1973, the long-term
11 trend of 1/Vis is 1.2% yr⁻¹ (p < 0.001), lying between the separated short-term trends. This
12 1/Vis trend evolution resembles the SO₂ emission trend. Industrial activity gradually
13 decreased after World War II until mid 1950s, followed by economic growth until the early
14 1970s with the emergence of both the oil crisis and the Clean Air Act (Greenstone, 2001). The
15 emission of SO₂ starts to consistently decrease after 1973 for the Smith inventory, and after
16 1977 for the EDGAR inventory. For the period 1973-1980 the regional 1/Vis is generally
17 consistent with these two inventories except for an anomalous peak of annual 1/Vis in 1977-
18 1979. The NOAA Climate Extremes Index (<http://www.ncdc.noaa.gov/extremes/cei/>)
19 describes the winters of 1977-1979 as the coldest during 1945-1996 across the US. Increased
20 emissions from domestic heating, as well as stagnant weather may contribute to the 1/Vis
21 peak. After 1978, the three annual time series uniformly exhibit a downward tendency.

22 Table 1 contains the correlation of annual 1/Vis with SO₂ emissions. Annual 1/Vis over the
23 eastern US exhibits a correlation of 0.66 with the Smith SO₂ emissions over the entire US
24 (1946-1995), and of 0.73 with the EDGAR SO₂ emissions over the eastern US (1970-1995).
25 The 1/Vis trends over the western US (where SO₂ emissions are much lower than in the
26 Eastern US, organic aerosols dominate in PM_{2.5} and forest fires are more prevalent) are less
27 consistent than over the eastern US with the SO₂ emission data, given the influence of other
28 sources. In summary, the 1/Vis time series successfully capture large-scale haze evolution
29 over the eastern US from 1945 to 1996, which is consistent with changes in SO₂ emissions as
30 well as previous investigations on 1/Vis for this region (Husar and Wilson, 1993; Schichtel et
31 al., 2001).

1 Figure A4 shows the calculated $1/\text{Vis}$ trends over the US for two short periods prior to 1945.
2 Although the stations are sparsely distributed, the nearly uniform trends in $1/\text{Vis}$ strongly
3 suggest a prominent decrease over 1929-1934, and then a rapid increase over 1935-1944. This
4 evolution reflects the significant drop in industrial activity following the 1929 Great
5 Depression, and the economic recovery after \sim 1933 during the New Deal programs and
6 World War II. The Smith SO_2 emissions of the US (Fig. A3) also reflect these socioeconomic
7 events.

8 **5.2 Europe**

9 Figure 9 presents the spatial distribution and temporal evolution of haze trends over Europe as
10 derived from the $1/\text{Vis}$ data for 1973-2005. The historical trend pattern of $1/\text{Vis}$ is quite
11 different between Western and Eastern Europe. The large-scale $1/\text{Vis}$ trend over Western
12 Europe is consistently decreasing for the 4 periods after 1981 (also in Fig. 5). Some countries
13 such as the UK and France begin decreasing prior to 1981, consistent with the SO_2 emission
14 decrease over these countries (Fig. A3). Prior analysis also indicated Vis improvements after
15 \sim 1973 for most sites over the UK (Doyle and Dorling, 2002). Meanwhile stations over
16 Eastern Europe have significantly increased $1/\text{Vis}$ for 1973-1980, a mostly decreasing trend in
17 its western part for 1981-1988, and then a decrease-dominant trend after 1989.

18 Figure 10 shows the regionally composite time series of $1/\text{Vis}$ as well as SO_2 emissions over
19 Western and Eastern Europe for 1973-2013. Table 2 lists the specific country names included
20 in the Smith emissions for the two regions. The evolution of $1/\text{Vis}$ over Western and Eastern
21 Europe is broadly consistent with the SO_2 emissions, and reflects the lag of emission
22 reduction in Eastern versus Western Europe. Stjern et al. (2011) similarly reported later
23 improvement in Vis over Eastern versus Western Europe. The SO_2 emission reduction
24 extends from the 1980s to the end of data record for Western Europe, and primarily over
25 1989-2000 for Eastern Europe. The composite $1/\text{Vis}$ time series successfully capture the
26 significant reduction of haze over Western Europe (-1.1 to -1.7% yr^{-1} , $p < 0.08$). Long term
27 $1/\text{Vis}$ trend over Western Europe for 1981-2011 (insufficient qualified stations after 2011) is -
28 1.8% yr^{-1} ($p < 0.001$), consistent with the separate short-term trends. For Eastern Europe the
29 decrease of $1/\text{Vis}$ is stronger before 1997 (-2.0% yr^{-1} , $p < 0.001$) than after 2006 (-1.1% yr^{-1} , p
30 $= 0.03$), and the calculated trend over 1997-2005 is insignificant, consistent with the SO_2
31 emission evolution. There is an obvious peak in $1/\text{Vis}$ from October 1995 to March 1996

1 especially over Eastern Europe, which is consistent with the peak sulfate concentration that
2 Stjern et al. (2011) attributed to the anomalously cold winter of 1996 with stagnant air.
3 Table 1 shows that the annual $1/\text{Vis}$ time series exhibit a correlation of 0.91 (0.92) with the
4 Smith Emissions for 1973-2005, and of 0.92 (0.92) with the EDGAR emissions for 1973-
5 2008 over Western (Eastern) Europe, respectively. Such high correlations suggest a major
6 role of SO_2 emissions to determine the decadal trends of haze over Europe.

7 **5.3 Eastern Asia**

8 Figure 11 shows the calculated relative trends of $1/\text{Vis}$ over Eastern Asia after 1973. A
9 persistent increasing trend of $1/\text{Vis}$ dominates over eastern China for more than 30 years. A
10 prominent feature in the trends over China is more heterogeneity in the spatial distribution
11 compared to the trend maps over the US and Europe. This could be a result of asynchronous
12 economic development, as several studies reported “lagging” of Vis impairment in rural sites
13 (from ~1990s) compared to urban sites (from ~1960s) in China (Quan et al., 2011; Wu et al.,
14 2012). The overall increasing trend in $1/\text{Vis}$ reverses in the last period of 2006-2013, when
15 most stations in southern China and many in northern China show a statistically significant
16 decreasing trend of $1/\text{Vis}$. This is consistent with the implementation of fuel-gas
17 desulfurization facilities in power plants after ~2007. This recent reduction was also
18 supported by satellite observations of SO_2 (Li et al., 2010; Lu et al., 2010; Lu et al., 2011; S.
19 Wang et al., 2015; Zhao et al., 2013).

20 Figure 11 also shows a consistent increase of $1/\text{Vis}$ over Korea from 1973 to 1996. After 1997
21 when the SO_2 emission transits to decrease (Fig. A3), the increase in $1/\text{Vis}$ levels off and
22 reverses. The aerosols over China also affect areas downwind through long-range transport
23 (Aikawa et al., 2010). For the 1997-2005 period, most eastern stations of Korea show a
24 downward trend, in contrast with the increasing $1/\text{Vis}$ over the west, which is more strongly
25 influenced by pollutant transport from China. Lee et al. (2015) also discovered insignificant
26 improvement of Vis over urban areas of Korea after late 1990s despite the national emission
27 reduction policy launched in early 2000s, which was attributed to the regional transport from
28 upwind continental areas. Long-term aerosol measurement over Gosan Island, Korea showed
29 rapid increase of sulfate and nitrate concentrations from early 2000s to ~2006, which were
30 closely related with the trends of China’s emission (Kim et al., 2011). Similarly, stations over
31 the western and coastal areas of Japan consistently exhibit an upward $1/\text{Vis}$ trend before 2006,

1 despite the continuous decrease of local SO₂ emission and concentration since 1970
2 (Wakamatsu et al., 2013). Aikawa et al. (2010) found a zonal gradient in terms of both the
3 magnitude and trend of measured SO₂ and sulfate concentrations over Japan, and in the
4 modeled contribution from China to the sulfate concentration in Japan. Lu et al. (2010)
5 reported that most EANET (Acid Deposition Monitoring Network in East Asia) stations over
6 Japan and Korea have increasing trends in SO₂ and sulfate aerosols from 2001 to 2007. For
7 the last period 2006-2013, 1/Vis shows a dominant decreasing trend over Japan and Korea
8 that may reflect in part China's SO₂ emission controls. Itahashi et al. (2012) reported a trend
9 reversal of MODIS (Moderate Resolution Imaging Spectroradiometer) fine aerosol optical
10 depth (AOD) over the Sea of Japan from increasing to decreasing at ~2006 that is more
11 consistent with China's SO₂ emission than the local emission. This analysis highlights the
12 sensitivity of 1/Vis to long range transport, and the value of international collaboration for air
13 quality improvement over Eastern Asia.

14 Figure 12 presents a regional analysis of averaged 1/Vis time series over northern and
15 southern China, and the evolution of SO₂ emissions from two inventories. The overall Vis
16 impairment trend in China for 1973-2005 reflects the consistent SO₂ emission increase. Both
17 the north and south show a steady and significant ($p < 0.001$) increase of haziness for the
18 1973-1980 period, and southern China shows an even faster impairment (2.9% yr⁻¹) than the
19 north (1.2% yr⁻¹). For the next 2 decades (1980-2000) the 1/Vis increase slows down in both
20 the south and the north, in accordance with other investigations using Vis and SSR data (Chen
21 and Wang, 2015; Luo et al., 2001; Wu et al., 2014). The south exhibits a slower (0.2% yr⁻¹)
22 and less significant ($p > 0.3$) increase than the north (0.5–0.6% yr⁻¹). The long-term trend over
23 1981-1996 for Northern China (0.5% yr⁻¹, $p < 0.001$) also exceeds that for Southern China
24 (0.2% yr⁻¹, $p = 0.04$). This difference is determined not only by the slower increase of SO₂
25 emissions in the south (Lu et al., 2010), but also by more precipitation and ventilation in the
26 south that favors the removal of aerosols and their precursors (Xu, 2001; Ye et al., 2013). The
27 decline of SO₂ emissions from 1996 to 2000 reflects both the 1997 Asian financial crisis, and
28 a decline in coal use and sulfur content (Lu et al., 2011). Both regions show a leveling off or
29 even reversal of 1/Vis increase during this short period, which is again more significant in the
30 south. The period 2000-2006 exhibits significant growth (>1% yr⁻¹) of 1/Vis in both the north
31 and south, resembling the steady growth in SO₂ emissions. The recent reduction of SO₂
32 emissions is reflected in the Lu emissions while not in the EDGAR emissions. After 2006
33 significant ($p < 0.05$) decreasing trends in 1/Vis are apparent (-0.9 to -1.6% yr⁻¹) for both

1 northern and southern China, which is more consistent with the Lu emissions. As shown in
2 Table 1, the annual 1/Vis time series exhibit a high correlation of 0.78 (0.87) with the Lu
3 emissions (1996-2010), and of 0.91 (0.88) with the EDGAR emissions (1973-2008) over
4 northern (southern) China, respectively.

5 **5.4 Connections to SSR and AOD trends**

6 Long-term records of surface solar radiation (SSR) and columnar aerosol optical depth (AOD)
7 serve as complimentary data resources to study and interpret changes in air pollution during
8 the last few decades, especially for regions with fewer ground-based aerosol measurements.
9 SSR is determined by the total columnar extinction of aerosols and clouds while 1/Vis
10 represents the extinction level at the surface. Moreover, the direct scattering and absorption of
11 solar radiation by aerosols could be amplified in less polluted regions or dampened over
12 highly polluted stations, due to aerosol-cloud interaction (Fuzzi et al., 2015; Wild, 2009).
13 Despite these uncertainties, the observed reversals of SSR from “dimming” to “brightening”
14 in 1980-1990 over the US and Europe (Streets et al., 2006; Turnock et al., 2015; Wild, 2012)
15 generally agree with the reversals around the 1980s of 1/Vis trends in this study. Over China,
16 the recently reported decadal SSR variation shows dimming before the 1990s and no
17 significant trend afterwards (Tang et al., 2011; K. Wang et al., 2015). The latter phenomenon
18 may reflect compensation of more aerosol extinction by less cloud cover (Norris and Wild,
19 2009).

20 Reliable AOD data over land are limited to the recent two decades, but exhibit even greater
21 consistency with 1/Vis trends. The recent decrease in 1/Vis after late-1990s over the US and
22 Western Europe in this study is consistent with previous studies on AOD trends based on both
23 ground based (e.g. Li et al., 2014; Yoon et al., 2012) and satellite (e.g. Chin et al., 2014; Hsu
24 et al., 2012; Pozzer et al., 2015) observations. Over China, several studies on AOD trends in
25 the 2000s showed notable increasing tendency (e.g. Hsu et al., 2012; Pozzer et al., 2015;
26 Yoon et al., 2012), while some recent studies also discovered that separating AOD time series
27 could reflect the plateauing and reversal of trends in recent years due to emission control
28 strategies (Che et al., 2015; He et al., 2016; Lu et al., 2011). PM_{2.5} trends derived from
29 satellite AOD over 1998-2012 have decreasing tendencies over North America and Europe,
30 and increasing tendencies over Eastern Asia (Boys et al., 2014; Van Donkelaar et al., 2015),
31 similar to the 1/Vis trends found here.

1

2 **6 Conclusion**

3 This study examines Vis observations as a trend indicator of haziness and air quality over the
4 US (1945-1996), Europe (1973-2013), and Eastern Asia (1973-2013). We comprehensively
5 process the raw data from over 20,000 stations considering effects from meteorological
6 factors, protocol design, and human errors. We develop filters to exclude relatively clean
7 cases (i.e. months with $\leq 50\%$ records below the threshold Vis, or years with annual $1/\text{Vis} \leq$
8 40 Mm^{-1}) with weaker sensitivity to b_{ext} variation, and apply change point detection and
9 separation to largely reduce the intrinsic discontinuities. Nearly 4000 stations remain after the
10 processing with 753 over the US, 1625 over Europe, and 791 over Eastern Asia. The
11 composite time series of $1/\text{Vis}$ over the US for 1989-1996 generally agrees with the
12 collocated IMPROVE b_{ext} in terms of both seasonal variation ($r = 0.77$) and trends ($-1.6\% \text{ yr}^{-1}$,
13 $95\% \text{ CI: } -2.4, -0.8\% \text{ yr}^{-1}$) in $1/\text{Vis}$ versus b_{ext} ($-2.4\% \text{ yr}^{-1}$, $95\% \text{ CI: } -3.7, -1.1\% \text{ yr}^{-1}$). Similarly,
14 for 2006-2013 over Europe, the seasonal variation ($r = 0.80$) and significant decrease (-5.8%
15 yr^{-1} , $95\% \text{ CI: } -7.8, -4.2\% \text{ yr}^{-1}$) in $\text{PM}_{2.5}$ are captured by collocated $1/\text{Vis}$ ($-3.4\% \text{ yr}^{-1}$, $95\% \text{ CI:}$
16 $-4.4, -2.4\% \text{ yr}^{-1}$). This consistency highlights the benefits of thorough data screening to reduce
17 uncertainties brought by the inherent issues in Vis observations such as threshold choices,
18 discreteness and discontinuities. As discussed in Section 3.1, the inclusion of unresolved
19 values in the mean $1/\text{Vis}$ and the contaminants of discontinuities could dampen the ability of
20 $1/\text{Vis}$ to correctly resolve aerosol trends. Admittedly, the derived $1/\text{Vis}$ trends are still subject
21 to several uncertainties, e.g. the spatially variant K and data quality, the less robust short-term
22 trends, sampling differences and direct averaging in composite time series. Nevertheless, the
23 interpretation value of $1/\text{Vis}$ data is shown to be enhanced by the comprehensive screening
24 and spatial averaging. Therefore we focus on the trend results that are regionally coherent and
25 aggregated, and avoid drawing strong conclusions based solely on the $1/\text{Vis}$ trends. Although
26 at individual stations the $1/\text{Vis}$ changes might be affected by these above stated artificial
27 factors, regionally coherent trend signals suggest these derived $1/\text{Vis}$ trends represent actual
28 changes in b_{ext} . Our filtered monthly $1/\text{Vis}$ data are freely available as a public good
29 (http://fizz.phys.dal.ca/~atmos/martin/?page_id=2527).

30 Analysis of the $1/\text{Vis}$ trends for several short periods reveals haze trend evolution and
31 reversals. These historical $1/\text{Vis}$ trends and their evolution also exhibit compelling
32 consistency with SO_2 emissions and SSR studies. For example, $1/\text{Vis}$ shows statistically

1 significant decreasing trends from the late 1970s to the mid 1990s over the eastern US (-1.1 to
2 -2.0% yr⁻¹), from the early 1980s to 2013 over Western Europe (-1.1 to -1.7% yr⁻¹), in the
3 early 1990s (-2.0% yr⁻¹) and after the mid 2000s (-1.1% yr⁻¹) over Eastern Europe, and after
4 the mid 2000s over China (-0.9 to -1.6%/yr). These recent decreases in 1/Vis are attributable
5 to emission changes in these populated areas. Reversal points of 1/Vis trends also consistently
6 reflect several historical socioeconomic events e.g. the New Deal programs (from decrease to
7 increase at ~1934), the end of World War II (from increase to decrease at ~1945) and the
8 Clean Air Act (from increase to decrease at ~1979) in the US, the collapse of communism in
9 Eastern Europe (from increase to decrease at ~1989), and the 1997 Asian financial crisis.

10 Therefore, the constructed 1/Vis data are applicable to resolve historical aerosol trends on a
11 regional and annual basis, and provide complementary information about the historical
12 changes in air quality. For instance, the annual 1/Vis time series exhibit high correlations
13 (0.7-0.9) with SO₂ emissions for 5 large domains (Table 1). Apart from verifying the
14 historical 1/Vis trends, this consistency also provides an evaluation of emission inventories.
15 For example, after ~2006 1/Vis trends agree better with Lu et al. (2011) than the EDGAR
16 emissions in capturing the SO₂ emission controls over China. Emission inventories differ
17 significantly (S. Smith et al., 2011a), and 1/Vis data offer constraints on these inventories.

18 However, SO₂ emission inventories cannot fully explain the trends in ambient haze due to the
19 influence of other emissions and meteorological factors. Notable reductions in emissions of
20 nitrogen oxides and black carbon have been reported over North America and Western
21 Europe (Bond et al., 2007; Lu et al., 2015; US EPA, 2012; Vestreng et al., 2009), while
22 steady increase in emissions of nitrogen oxides, organic carbon and black carbon were
23 identified over China (Lu et al., 2011; Zhao et al., 2013). Observed (Leibensperger et al.,
24 2012; Murphy et al., 2011) and simulated (Lin et al., 2010; Wang et al., 2013) changes in
25 various aerosol chemical species suggest increasing importance of emissions other than SO₂
26 on air quality trends in recent years. We have also shown that occasional cold winters in the
27 US and Europe, and the long-range transport of China's pollutants into Korea and Japan could
28 affect the association between 1/Vis and local emission. Future work includes applying a
29 chemical transport model to further interpret the observed 1/Vis (*b_{ext}*) trends, as well as the
30 contribution from meteorology and emissions.

31

32 **Appendix**

1 Four appendix figures (Fig. A1-A4) are included for complementary interpretation.

2

3 **Acknowledgements**

4 This work is supported by the Natural Science and Engineering Research Council of Canada.
5 C. Li is partially supported by a Killiam Predoctoral Scholarship, and an ACEnet Research
6 Fellowship. We thank two anonymous reviewers for their helpful comments. Special thanks
7 to Dr. Jing Li at NASA GISS for instructions and discussion about trend calculation, Dr.
8 Xiaolan Wang and Dr. Yang Feng at Climate Research Division, Environment Canada for
9 maintaining the RHtest software, and Dr. Zifeng Lu at Argonne National Laboratory for
10 guidance in SO₂ emission data. This work primarily relies on the visibility data provided by
11 NOAA NCEI. The b_{ext} data are from the IMPROVE network. IMPROVE is a collaborative
12 association of state, tribal, and federal agencies, and international partners. US Environmental
13 Protection Agency is the primary funding source, with contracting and research support from
14 the National Park Service. The Air Quality Group at the University of California, Davis is the
15 central analytical laboratory, with ion analysis provided by Research Triangle Institute, and
16 carbon analysis provided by Desert Research Institute. We acknowledge the EMEP
17 measurement networks and the data managers for maintaining the PM_{2.5} data for validating
18 1/Vis trends over Europe. We also thank NASA SEDAC and EDGAR for making the
19 emission data used in this study publicly available.

20

1 **References**

- 2 Aas, W., Tsyro, S., Bieber, E., Bergström, R., Ceburnis, D., Ellermann, T., Fagerli, H.,
3 Frölich, M., Gehrig, R., Makkonen, U., Nemitz, E., Otjes, R., Perez, N., Perrino, C., Prévôt,
4 A. S. H., Putaud, J.-P., Simpson, D., Spindler, G., Vana, M., and Yttri, K. E.: Lessons learnt
5 from the first EMEP intensive measurement periods, *Atmos. Chem. Phys.*, 12, 8073-8094,
6 2012.
- 7 Aikawa, M., Ohara, T., Hiraki, T., Oishi, O., Tsuji, A., Yamagami, M., Murano, K., and
8 Mukai, H.: Significant geographic gradients in particulate sulfate over Japan determined from
9 multiple-site measurements and a chemical transport model: Impacts of transboundary
10 pollution from the Asian continent, *Atmos. Environ.*, 44, 381-391, 2010.
- 11 Apte, J. S., Marshall, J. D., Cohen, A. J., and Brauer, M.: Addressing Global Mortality from
12 Ambient PM_{2.5}. *Environ. Sci. Technol.*, 49, 8057-8066, 2015.
- 13 Attwood, A., Washenfelder, R., Brock, C., Hu, W., Baumann, K., Campuzano - Jost, P., Day,
14 D., Edgerton, E., Murphy, D., and Palm, B.: Trends in sulfate and organic aerosol mass in the
15 Southeast US: Impact on aerosol optical depth and radiative forcing, *Geophys. Res. Lett.*, 41,
16 7701-7709, 2014.
- 17 Ayers, G. P.: Comment on regression analysis of air quality data. *Atmos. Environ.*, 35(13),
18 2423-2425, 2001.
- 19 Brauer, M., Amann, M., Burnett, R. T., Cohen, A., Dentener, F., Ezzati, M., Henderson, S. B.,
20 Krzyzanowski, M., Martin, R. V., Van Dingenen, R., van Donkelaar, A., and Thurston, G. D.:
21 Exposure assessment for estimation of the global burden of disease attributable to outdoor air
22 pollution. *Environ. Sci. Technol.*, 48, 652-660, 2012.
- 23 Bond, T. C., Bhardwaj, E., Dong, R., Jogani, R., Jung, S., Roden, C., Streets, D. G., and
24 Trautmann, N. M.: Historical emissions of black and organic carbon aerosol from energy-
25 related combustion, 1850–2000, *Global Biogeochem. Cy.*, 21, GB2018,
26 doi:10.1029/2006GB002840, 2007.
- 27 Boys, B., Martin, R., van Donkelaar, A., MacDonell, R., Hsu, N., Cooper, M., Yantosca, R.,
28 Lu, Z., Streets, D. G., and Zhang, Q.: Fifteen-Year Global Time Series of Satellite-Derived
29 Fine Particulate Matter, *Environ. Sci. Technol.*, 48, 11109-11118, 2014.

1 Che, H., Zhang, X., Li, Y., Zhou, Z., and Qu, J. J.: Horizontal visibility trends in China 1981–
2 2005, *Geophys. Res. Lett.*, 34, L24706, doi:10.1029/2007GL031450, 2007.

3 Che, H., Zhang, X.-Y., Xia, X., Goloub, P., Holben, B., Zhao, H., Wang, Y., Zhang, X.-C.,
4 Wang, H., Blarel, L., Damiri, B., Zhang, R., Deng, X., Ma, Y., Wang, T., Geng, F., Qi, B.,
5 Zhu, J., Yu, J., Chen, Q., and Shi, G.: Ground-based aerosol climatology of China: aerosol
6 optical depths from the China Aerosol Remote Sensing Network (CARSNET) 2002–2013,
7 *Atmos. Chem. Phys.*, 15, 7619-7652, doi:10.5194/acp-15-7619-2015, 2015.

8 Chen, H. and Wang, H.: Haze days in North China and the associated atmospheric
9 circulations based on daily visibility data from 1960 to 2012, *J. Geophys. Res.*, 120, 5895–
10 5909, doi:10.1002/2015JD023225, 2015.

11 Chen, Y., Zheng, M., Edgerton, E. S., Ke, L., Sheng, G., and Fu, J.: PM2.5 source
12 apportionment in the southeastern US: spatial and seasonal variations during 2001–2005, *J.*
13 *Geophys. Res.*, 117, D08304, doi:10.1029/2011JD016572, 2012.

14 Chin, M., Diehl, T., Tan, Q., Prospero, J., Kahn, R., Remer, L., Yu, H., Sayer, A., Bian, H.,
15 and Geogdzhayev, I.: Multi-decadal variations of atmospheric aerosol from 1980-2009:
16 Sources and regional trends, *Atmos. Chem. Phys.*, 14, 3657-3690, 2014.

17 Chin, M., Jacob, D. J., Gardner, G. M., Foreman - Fowler, M. S., Spiro, P. A., and Savoie, D.
18 L.: A global three - dimensional model of tropospheric sulfate, *J. Geophys. Res.*, 101, 18667-
19 18690, 1996.

20 Collaud Coen, M., Andrews, E., Asmi, A., Baltensperger, U., Bukowiecki, N., Day, D.,
21 Fiebig, M., Fjaeraa, A., Flentje, H., and Hyvärinen, A.: Aerosol decadal trends–Part 1: In-situ
22 optical measurements at GAW and IMPROVE stations, *Atmos. Chem. Phys.*, 13, 869-894,
23 2013.

24 Costa, A. C., and Soares, A.: Homogenization of climate data: review and new perspectives
25 using geostatistics, *Math. Geosci.*, 41, 291-305, 2009.

26 Denier van der Gon, H. A. C., Bergström, R., Fountoukis, C., Johansson, C., Pandis, S. N.,
27 Simpson, D., and Visschedijk, A. J. H.: Particulate emissions from residential wood
28 combustion in Europe – revised estimates and an evaluation, *Atmos. Chem. Phys.*, 15, 6503-
29 6519, 2015

1 Doyle, M., and Dorling, S.: Visibility trends in the UK 1950–1997. *Atmos. Environ.*, 36,
2 3161-3172, 2002.

3 Daum, P. H., Schwartz, S. E., and Newman, L.: Acidic and related constituents in liquid water
4 stratiform clouds, *J. Geophys. Res.*, 89, 1447-1458, 1984.

5 EC-JRC/PBL (European Commission, Joint Research Center/Netherlands Environmental
6 Assessment Agency): Emission Database for Global Atmospheric Research (EDGAR),
7 release version 4.2, available at: <http://edgar.jrc.ec.europa.eu>, 2011.

8 Fuzzi, S., Baltensperger, U., Carslaw, K., Decesari, S., Denier van der Gon, H., Facchini, M.
9 C., et al.: Particulate matter, air quality and climate: lessons learned and future needs, *Atmos.*
10 *Chem. Phys.*, 15, 8217-8299, 2015.

11 Greenstone, M.: The Impacts of Environmental Regulations on Industrial Activity: Evidence
12 from the 1970 and 1977 Clean Air Act Amendments and the Census of Manufactures, *J. Polit.*
13 *Econ.*, 110, 1175-1219, 2001.

14 Griffing, G. W.: Relations between the prevailing visibility, nephelometer scattering
15 coefficient and sunphotometer turbidity coefficient, *Atmos. Environ.*, 14, 577-584, 1980.

16 Hand, J. L., Schichtel, B. A., Malm, W. C., and Pitchford, M. L.: Particulate sulfate ion
17 concentration and SO₂ emission trends in the United States from the early 1990s through
18 2010, *Atmos. Chem. Phys.*, 12, 10353-10365, 2012a.

19 Hand, J. L., Schichtel, B. A., Malm, W. C., Copeland, S., Molenaar, J. V., Frank, N., and
20 Pitchford, M.: Widespread reductions in haze across the United States from the early 1990s
21 through 2011, *Atmos. Environ.*, 94, 671–679, 2014.

22 Hand, J., Schichtel, B., Pitchford, M., Malm, W., and Frank, N.: Seasonal composition of
23 remote and urban fine particulate matter in the United States, *J. Geophys. Res.*, 117, D05209,
24 doi:10.1029/2011JD017122, 2012b.

25 He, Q., Zhang, M., and Huang, B.: Spatio-temporal variation and impact
26 factors analysis of satellite-based aerosol optical depth over China from 2002 to 2015, *Atmos.*
27 *Environ.*, doi: 10.1016/j.atmosenv.2016.01.002., 2016.

28 Hsu, N. C., Gautam, R., Sayer, A. M., Bettenhausen, C., Li, C., Jeong, M. J., Tsay, S.-C., and
29 Holben, B. N.: Global and regional trends of aerosol optical depth over land and ocean using
30 SeaWiFS measurements from 1997 to 2010, *Atmos. Chem. Phys.*, 12, 8037-8053, 2012.

1 Husar, R. B., Holloway, J. M., Patterson, D. E., and Wilson, W. E.: Spatial and temporal
2 pattern of eastern US haziness: a summary, *Atmos. Environ.*, 15, 1919-1928, 1981.

3 Husar, R. B. and Patterson, D. E.: Haze Climate of the United States: Project Summary, U.S.
4 Environmental Protection Agency, EPA-600/S3-86-071, available at:
5 <http://nepis.epa.gov/Exe/ZyPDF.cgi/4000173E.PDF?Dockey=4000173E.PDF>, last access: 29
6 April 2015, 1987.

7 Husar, R. B., and Wilson, W. E.: Haze and sulfur emission trends in the eastern United States,
8 *Environ. Sci. Technol.*, 27, 12-16, 1993.

9 Husar, R. B., Husar, J. D., and Martin, L.: Distribution of continental surface aerosol
10 extinction based on visual range data, *Atmos. Environ.*, 34, 5067-5078, 2000.

11 Intergovernmental Panel on Climate Change (IPCC), *Climate Change 2013: The Physical
12 Science Basis*, Cambridge Univ. Press, Cambridge, 2013.

13 Itahashi, S., Uno, I., Yumimoto, K., Irie, H., Osada, K., Ogata, K., Fukushima, H., Wang, Z.,
14 and Ohara, T.: Interannual variation in the fine-mode MODIS aerosol optical depth and its
15 relationship to the changes in sulfur dioxide emissions in China between 2000 and 2010,
16 *Atmos. Chem. Phys.*, 12, 2631-2640, 2012.

17 Kendall, M. G.: *Rank Correlation Methods*, Griffin, London, 1975.

18 Kessner, A. L., Wang, J., Levy, R. C., and Colarco, P. R.: Remote sensing of surface visibility
19 from space: A look at the United States East Coast, *Atmos. Environ.*, 81, 136-147, 2013.

20 Kim, N. K., Kim, Y. P., and Kang, C. H.: Long-term trend of aerosol composition and direct
21 radiative forcing due to aerosols over Gosan: TSP, PM₁₀, and PM_{2.5} data between 1992 and
22 2008. *Atmos. Environ.*, 45, 6107-6115, 2011.

23 Lee, H.J., Kang, J.E. and Kim, C.H.: Forty year (1971–2010) semi-quantitative observations
24 of visibility-cloud-precipitation in Korea and its implication for aerosol effects on regional
25 climate, *J. Air Waste Ma.*, 65, 788-799, doi:10.1080/10962247.2015.1016633, 2015.

26 Leibensperger, E., Mickley, L. J., Jacob, D. J., Chen, W.-T., Seinfeld, J., Nenes, A., Adams,
27 P., Streets, D., Kumar, N., and Rind, D.: Climatic effects of 1950–2050 changes in US
28 anthropogenic aerosols–Part 1: Aerosol trends and radiative forcing, *Atmos. Chem. Phys.*, 12,
29 3333-3348, 2012.

1 Li, C., Zhang, Q., Krotkov, N. A., Streets, D. G., He, K., Tsay, S. C., and Gleason, J. F.:
2 Recent large reduction in sulfur dioxide emissions from Chinese power plants observed by the
3 Ozone Monitoring Instrument, *Geophys. Res. Lett.*, 37, L08807, doi:10.1029/2010GL042594,
4 2010.

5 Li, J., Carlson, B., Dubovik, O., and Lacis, A.: Recent trends in aerosol optical properties
6 derived from AERONET measurements, *Atmos. Chem. Phys.*, 14, 12271-12289, 2014.

7 Lim, S. S., Vos, T., Flaxman, A. D., Danaei, G., Shibuya, K., Adair-Rohani, H., AlMazroa,
8 M. A., Amann, M., Anderson, H. R., Andrews, K. G., Aryee, M., Atkinson, C., Bacchus, L.
9 J., Bahalim, A. N., Balakrishnan, K., Balmes, J., Barker-Collo, S., Baxter, A., Bell, M. L.,
10 Blore, J. D., Blyth, F., Bonner, C., Borges, G., Bourne, R., Boussinesq, M., Brauer, M.,
11 Brooks, P., 15 Bruce, N. G., Brunekreef, B., Bryan-Hancock, C., Bucello, C., Buchbinder, R.,
12 Bull, F., Burnett, R. T., Byers, T. E., Calabria, B., Carapetis, J., Carnahan, E., Chafe, Z.,
13 Charlson, F., Chen, H., Chen, J. S., Cheng, A. T., Child, J. C., Cohen, A., Colson, K. E.,
14 Cowie, B. C., Darby, S., Darling, S., Davis, A., Degenhardt, L., Dentener, F., Des Jarlais, D.
15 C., Devries, K., Dherani, M., Ding, E. L., Dorsey, E. R., Driscoll, T., Edmond, K., Ali, S. E.,
16 Engell, R. E., Erwin, P. J., Fahimi, S., Falder, G., Farzadfar, F., Ferrari, A., Finucane, M. M.,
17 Flaxman, S., Fowkes, F. G. R., Freedman, G., Freeman, M. K., Gakidou, E., Ghosh, S.,
18 Giovannucci, E., Gmel, G., Graham, K., Grainger, R., Grant, B., Gunnell, D., Gutierrez, H.
19 R., Hall, W., Hoek, H. W., Hogan, A., Hosgood III, H. D., Hoy, D., Hu, H., Hubbell, B. J.,
20 Hutchings, S. J., Ibeanusi, S. E., Jacklyn, G. L., Jasrasaria, R., Jonas, J. B., Kan, H., Kanis, J.
21 A., Kassebaum, N., Kawakami, N., Khang, Y., Khatibzadeh, S., Khoo, J., Kok, C., Laden, F.,
22 Laloo, R., Lan, Q., Lathlean, T., Leasher, J. L., Leigh, J., Li, Y., Lin, J. K., Lipshultz, S. E.,
23 London, S., Lozano, R., Lu, Y., Mak, J., Malekzadeh, R., Mallinger, L., Marcenes, W.,
24 March, L., Marks, R., Martin, R., McGale, P., McGrath, J., Mehta, S., Memish, Z. A.,
25 Mensah, G. A., Merriman, T. R., Micha, R., Michaud, C., Mishra, V., Hanafiah, K. M.,
26 Mokdad, A. A., Morawska, L., Mozaffarian, D., Murphy, T., Naghavi, M., Neal, B., Nelson,
27 P. K., Nolla, J. M., Norman, R., Olives, C., Omer, S. B., Orchard, J., Osborne, R., Ostro, B.,
28 Page, A., Pandey, K. D., Parry, C. D., Passmore, E., Patra, J., Pearce, N., Pelizzari, P. M.,
29 Petzold, M., Phillips, M. R., Pope, D., Pope III, C. A., Powles, J., Rao, M., Razavi, H.,
30 Rehfuss, E. A., Rehm, J. T., Ritz, B., Rivara, F. P., Roberts, T., Robinson, C.,
31 RodriguezPortales, J. A., Romieu, I., Room, R., Rosenfeld, L. C., Roy, A., Rushton, L.,
32 Salomon, J. A., Sampson, U., Sanchez-Riera, L., Sanman, E., Sapkota, A., Seedat, S., Shi, P.,

- 1 Shield, K., Shivakoti, R., Singh, G. M., Sleet, D. A., Smith, E., Smith, K. R., Stapelberg, N.
2 J., Steenland, K., Stöckl, H., Stovner, L. J., Straif, K., Straney, L., Thurston, G. D., Tran, J.
3 H., Van Dingenen, R., van Donkelaar, A., Veerman, J. L., Vijayakumar, L., Weintraub, R.,
4 Weissman, M. M., White, R. A., Whiteford, H., Wiersma, S. T., Wilkinson, J. D., Williams,
5 H. C., Williams, W., Wilson, N., Woolf, A. D., Yip, P., Zielinski, J. M., Lopez, A. D.,
6 Murray, C. J., and Ezzati, M.: A comparative risk assessment of burden of disease and injury
7 attributable to 67 risk factors and risk factor clusters in 21 regions, 1990–2010: a systematic
8 analysis for the Global Burden of Disease Study 2010, *Lancet*, 380, 2224–2260,
9 doi:10.1016/S0140-6736(12)61766-8, 2012.
- 10 Lin, J., Nielsen, C. P., Zhao, Y., Lei, Y., Liu, Y., and McElroy, M. B.: Recent changes in
11 particulate air pollution over China observed from space and the ground: effectiveness of
12 emission control, *Environ. Sci. Technol.*, 44, 7771-7776, 2010.
- 13 Lin, J., van Donkelaar, A., Xin, J., Che, H., and Wang, Y.: Clear-sky aerosol optical depth
14 over Eastern China estimated from visibility measurements and chemical transport modeling,
15 *Atmos. Environ.*, 95, 258-267, 2014.
- 16 Lu, Z., Streets, D. G., de Foy, B., Lamsal, L. N., Duncan, B. N., and Xing, J.: Emissions of
17 nitrogen oxides from US urban areas: estimation from Ozone Monitoring Instrument
18 retrievals for 2005–2014, *Atmos. Chem. Phys.*, 15, 10367-10383, doi:10.5194/acp-15-10367-
19 2015, 2015.
- 20 Lu, Z., Streets, D. G., Zhang, Q., Wang, S., Carmichael, G. R., Cheng, Y. F., Wei, C., Chin,
21 M., Diehl, T., and Tan, Q.: Sulfur dioxide emissions in China and sulfur trends in East Asia
22 since 2000, *Atmos. Chem. Phys.*, 10, 6311-6331, 2010.
- 23 Lu, Z., Zhang, Q., and Streets, D. G.: Sulfur dioxide and primary carbonaceous aerosol
24 emissions in China and India, 1996–2010, *Atmos. Chem. Phys.*, 11, 9839-9864, 2011.
- 25 Luo, Y., Lu, D., Zhou, X., Li, W., and He, Q.: Characteristics of the spatial distribution and
26 yearly variation of aerosol optical depth over China in last 30 years, *J. Geophys. Res.*, 106,
27 14501-14513, 2001.
- 28 Mahowald, N., Ballantine, J., Feddema, J., and Ramankutty, N.: Global trends in visibility:
29 implications for dust sources, *Atmos. Chem. Phys.*, 7, 3309-3339, 2007.
- 30 Mann, H. B.: Nonparametric tests against trend, *Econometrica*, 13, 245–259, 1945.

1 Murphy, D., Chow, J., Leibensperger, E., Malm, W., Pitchford, M., Schichtel, B., Watson, J.,
2 and White, W.: Decreases in elemental carbon and fine particle mass in the United States,
3 *Atmos. Chem. Phys.*, 11, 4679-4686, 2011.

4 Norris, J. R., and Wild, M.: Trends in aerosol radiative effects over China and Japan inferred
5 from observed cloud cover, solar “dimming,” and solar “brightening”. *J. Geophys. Res.*, 114,
6 D00D15, doi:10.1029/2008JD011378, 2009.

7 Papadimas, C. D., Hatzianastassiou, N., Mihalopoulos, N., Querol, X., and Vardavas, I.:
8 Spatial and temporal variability in aerosol properties over the Mediterranean basin based on
9 6-year (2000–2006) MODIS data, *J. Geophys. Res.*, 113, D11205,
10 doi:10.1029/2007JD009189, 2008.

11 Philip, S., Martin, R. V., van Donkelaar, A., Lo, J. W.-H., Wang, Y., Chen, D., Zhang, L.,
12 Kasibhatla, P. S., Wang, S., and Zhang, Q.: Global chemical composition of ambient fine
13 particulate matter for exposure assessment, *Environ. Sci. Technol.*, 48, 13060-13068, 2014.

14 Pitchford, M., Malm, W., Schichtel, B., Kumar, N., Lowenthal, D., and Hand, J.: Revised
15 algorithm for estimating light extinction from IMPROVE particle speciation data, *J. Air
16 Waste Ma.*, 57, 1326-1336, 2007.

17 Pozzer, A., de Meij, A., Yoon, J., Tost, H., Georgoulias, A. K., and Astitha, M.: AOD trends
18 during 2001–2010 from observations and model simulations, *Atmos. Chem. Phys.*, 15, 5521-
19 5535, 2015.

20 Qu, W., Wang, J., Gao, S., and Wu, T.: Effect of the strengthened western Pacific subtropical
21 high on summer visibility decrease over eastern China since 1973, *J. Geophys. Res.*, 118,
22 7142-7156, 2013.

23 Quan, J., Zhang, Q., He, H., Liu, J., Huang, M., and Jin, H.: Analysis of the formation of fog
24 and haze in North China Plain (NCP), *Atmos. Chem. Phys.*, 11, 8205-8214, 2011.

25 Reeves, J., Chen, J., Wang, X. L., Lund, R., and Lu, Q. Q.: A review and comparison of
26 changepoint detection techniques for climate data, *J Appl. Meteorol. Clim.*, 46, 900-915,
27 2007.

28 Rosenfeld, D., Dai, J., Yu, X., Yao, Z., Xu, X., Yang, X., and Du, C.: Inverse relations
29 between amounts of air pollution and orographic precipitation, *Science*, 315, 1396-1398,
30 2007.

1 Schichtel, B. A., Husar, R. B., Falke, S. R., and Wilson, W. E.: Haze trends over the United
2 States, 1980–1995, *Atmos. Environ.*, 35, 5205-5210, 2001.

3 Sen, P. K.: Estimates of the regression coefficient based on Kendall's tau, *J. Am. Stat. Assoc.*,
4 63, 1379-1389, 1968.

5 Smith, A., Lott, N., and Vose, R.: The integrated surface database: Recent developments and
6 partnerships, *B. Am. Meteorol. Soc.*, 92, 704-708, 2011.

7 Smith, S. J., Aardenne, J. v., Klimont, Z., Andres, R. J., Volke, A., and Delgado Arias, S.:
8 Anthropogenic sulfur dioxide emissions: 1850–2005, *Atmos. Chem. Phys.*, 11, 1101-1116,
9 2011a.

10 Smith, S. J., van Aardenne, J., Klimont, Z., Andres, R. J., Volke, A., and Delgado Arias, S.:
11 Anthropogenic Sulfur Dioxide Emissions, 1850-2005: National and Regional Data Set by
12 Source Category, Version 2.86. Palisades, NY: NASA Socioeconomic Data and Applications
13 Center (SEDAC), doi:10.7927/H49884X9, 2011b.

14 Stern, D. I.: Reversal of the trend in global anthropogenic sulfur emissions, *Global*
15 *Environmental Change*, 16, 207-220, 2006.

16 Stjern, C. W., Stohl, A., and Kristjánsson, J. E.: Have aerosols affected trends in visibility and
17 precipitation in Europe?, *J. Geophys. Res.*, 116, D02212, doi:10.1029/2010JD014603, 2011.

18 Streets, D. G., Wu, Y., and Chin, M.: Two - decadal aerosol trends as a likely explanation of
19 the global dimming/brightening transition, *Geophys. Res. Lett.*, 33, L15806,
20 doi:10.1029/2006GL026471, 2006.

21 Tang, W.-J., Yang, K., Qin, J., Cheng, C. C. K., and He, J.: Solar radiation trend across China
22 in recent decades: a revisit with quality-controlled data, *Atmos. Chem. Phys.*, 11, 393-406,
23 2011.

24 Tørseth, K., Aas, W., Breivik, K., Fjæraa, A. M., Fiebig, M., Hjellbrekke, A. G., Lund Myhre,
25 C., Solberg, S., and Yttri, K. E.: Introduction to the European Monitoring and Evaluation
26 Programme (EMEP) and observed atmospheric composition change during 1972 - 2009,
27 *Atmos. Chem. Phys.*, 12, 5447-5481, doi:10.5194/acp-12-5447-2012, 2012.

28 Turnock, S. T., Spracklen, D. V., Carslaw, K. S., Mann, G. W., Woodhouse, M. T., Forster, P.
29 M., Haywood, J., Johnson, C. E., Dalvi, M., Bellouin, N., and Sanchez-Lorenzo, A.: Modelled

1 and observed changes in aerosols and surface solar radiation over Europe between 1960 and
2 2009, *Atmos. Chem. Phys.*, 15, 9477-9500, 2015.

3 US Environmental Protection Agency: Our Nation's Air – Status and Trends Through 2010,
4 Washington, DC, 2012.

5 van Donkelaar, A., Martin, R. V., Brauer, M., and Boys, B. L.: Use of satellite observations
6 for long-term exposure assessment of global concentrations of fine particulate matter,
7 *Environ. Health. Persp.*, 123,135-143, 2015.

8 Vautard, R., Yiou, P., and van Oldenborgh, G. J.: Decline of fog, mist and haze in Europe
9 over the past 30 years, *Nat. Geosci.*, 2, 115-119, 2009.

10 Vestreng, V., Ntziachristos, L., Semb, A., Reis, S., Isaksen, I. S. A., and Tarrasón, L.:
11 Evolution of NO_x emissions in Europe with focus on road transport control measures, *Atmos.*
12 *Chem. Phys.*, 9, 1503-1520, doi:10.5194/acp-9-1503-2009, 2009.

13 Wakamatsu, S., Morikawa, T., and Ito, A.: Air pollution trends in Japan between 1970 and
14 2012 and impact of urban air pollution countermeasures, *Asian Journal of Atmospheric*
15 *Environment*, 7, 177-190, 2013.

16 Wang, K., Dickinson, R. E., and Liang, S.: Clear sky visibility has decreased over land
17 globally from 1973 to 2007, *Science*, 323, 1468-1470, 2009.

18 Wang, K., Dickinson, R., Su, L., and Trenberth, K.: Contrasting trends of mass and optical
19 properties of aerosols over the Northern Hemisphere from 1992 to 2011, *Atmos. Chem. Phys.*,
20 12, 9387-9398, 2012.

21 Wang, K., Ma, Q., Li, Z., and Wang, J.: Decadal variability of surface incident solar radiation
22 over China: Observations, satellite retrievals, and reanalyses. *J. Geophys. Res.*, 120, 6500-
23 6514, 2015.

24 Wang, S., Zhang, Q., Martin, R. V., Philip, S., Liu, F., Li, M., Jiang, X., and He, K.: Satellite
25 measurements oversee China's sulfur dioxide emission reductions from coal-fired power
26 plants, *Environ. Res. Lett.*, 10, 114015, doi:10.1088/1748-9326/10/11/114015, 2015.

27 Wang, X. L., Wen, Q. H., and Wu, Y.: Penalized maximal t test for detecting undocumented
28 mean change in climate data series, *J Appl. Meteorol. Clim.*, 46, 916-931, 2007.

29 Wang, X. L.: Penalized maximal F test for detecting undocumented mean shift without trend
30 change, *J. Atmos. Ocean. Tech.*, 25, 368-384, 2008a.

1 Wang, X. L.: Accounting for autocorrelation in detecting mean shifts in climate data series
2 using the penalized maximal t or F test, *J Appl. Meteorol. Clim.*, 47, 2423-2444, 2008b.

3 Wang, Y., Zhang, Q. Q., He, K., Zhang, Q., and Chai, L.: Sulfate-nitrate-ammonium aerosols
4 over China: response to 2000–2015 emission changes of sulfur dioxide, nitrogen oxides, and
5 ammonia, *Atmos. Chem. Phys.*, 13, 2635-2652, doi:10.5194/acp-13-2635-2013, 2013.

6 Weatherhead, E. C., Reinsel, G. C., Tiao, G. C., Meng, X. L., Choi, D., Cheang, W. K.,
7 Keller, T., DeLuisi, J., Wuebbles, D. J., and Kerr, J. B.: Factors affecting the detection of
8 trends: Statistical considerations and applications to environmental data, *J. Geophys. Res.*,
9 103, 17149-17161, 1998.

10 Wild, M., Gilgen, H., Roesch, A., Ohmura, A., Long, C. N., Dutton, E. G., Forgan, B., Kallis,
11 A., Russak, V., and Tsvetkov, A.: From dimming to brightening: Decadal changes in solar
12 radiation at Earth's surface, *Science*, 308, 847-850, 2005.

13 Wild, M.: Global dimming and brightening: A review, *J. Geophys. Res.*, 114, D00D16,
14 doi:10.1029/2008JD011470, 2009.

15 Wild, M.: Enlightening global dimming and brightening, *B. Am. Meteorol. Soc.*, 93, 27-37,
16 2012.

17 Willett, K. M., Williams Jr, C. N., Dunn, R. J., Thorne, P. W., Bell, S., Podesta, M. d., Jones,
18 P. D., and Parker, D. E.: HadISDH: an updateable land surface specific humidity product for
19 climate monitoring, *Clim. Past*, 9, 657-677, 2013.

20 WMO: Guide to Meteorological Instruments and Methods of Observation. Chapter 9.
21 Measurement of Visibility, I.9-1–I.9-15, WMO-No. 8, World Meteorological Organization,
22 Geneva, Switzerland, 2008.

23 Wong, E. Y., Gohlke, J., Griffith, W. C., Farrow, S., and Faustman, E. M.: Assessing the
24 health benefits of air pollution reduction for children. *Environ. Health. Persp.*, 112, 226–232,
25 2004.

26 Wu, J., Fu, C., Zhang, L., and Tang, J.: Trends of visibility on sunny days in China in the
27 recent 50 years, *Atmos. Environ.*, 55, 339-346, 2012.

28 Wu, J., Luo, J., Zhang, L., Xia, L., Zhao, D., and Tang, J.: Improvement of aerosol optical
29 depth retrieval using visibility data in China during the past 50 years, *J. Geophys. Res.*, 119,
30 13,370-313,387, 2014.

1 Xu, Q.: Abrupt change of the mid-summer climate in central Eastern China by the influence
2 of atmospheric pollution, *Atmos. Environ.*, 35, 5029-5040, 2001.

3 Xu, X., Wang, J., Henze, D. K., Qu, W., and Kopacz, M.: Constraints on aerosol sources
4 using GEOS - Chem adjoint and MODIS radiances, and evaluation with multisensor (OMI,
5 MISR) data. *J. Geophys. Res.*, 118, 6396-6413, 2013.

6 Ye, J., Li, W., Li, L., and Zhang, F.: “North drying and south wetting” summer precipitation
7 trend over China and its potential linkage with aerosol loading, *Atmos. Res.*, 125, 12-19,
8 2013.

9 Yoon, J., von Hoyningen-Huene, W., Kokhanovsky, A. A., Vountas, M., and Burrows, J. P.:
10 Trend analysis of aerosol optical thickness and Ångström exponent derived from the global
11 AERONET spectral observations, *Atmos. Meas. Tech.*, 5, 1271-1299, doi:10.5194/amt-5-
12 1271-2012, 2012.

13 Yttri, K. E., Aas, W., Tørseth, K., Kristiansen, N. I., Lund Myhre, C., Tsyro, S., Simpson, D.,
14 Bergström, R., Mareckova, K., Wankmuller, R., Klimont, Z., Ammann, M., Kouvarakis, G.,
15 Laj, P., Pappalardo, G., and Prévôt, A. S. H.: Transboundary particulate matter in Europe,
16 EMEP Status report, 4/2012, Joint CCC, MSC-W, CEIP and CIAM Report, available at: [http:
17 25 //www.nilu.no/projects/ccc/reports/emep4-2012.pdf](http://www.nilu.no/projects/ccc/reports/emep4-2012.pdf), last access: 14 October 2015, 2012.

18 Yue, S., Pilon, P., Phinney, B., and Cavadias, G.: The influence of autocorrelation on the
19 ability to detect trend in hydrological series, *Hydrol. Process.*, 16, 1807-1829, 2002.

20 Zhang, J., and Reid, J.: A decadal regional and global trend analysis of the aerosol optical
21 depth using a data-assimilation grade over-water MODIS and Level 2 MISR aerosol products,
22 *Atmos. Chem. Phys.*, 10, 10949-10963, 2010.

23 Zhao, Y., Zhang, J., and Nielsen, C.: The effects of recent control policies on trends in
24 emissions of anthropogenic atmospheric pollutants and CO₂ in China, *Atmos. Chem. Phys.*,
25 13, 487-508, 2013.

26

1 Table 1. Summary of Pearson correlation coefficients (r) between annual 1/Vis and SO₂
 2 emissions for 5 regions.

Inventory	Period	Eastern US	
Smith	1946-1995	0.66	
EDGAR	1970-2008	0.73	
		Eastern Europe	Western Europe
Smith	1973-2005	0.92	0.91
EDGAR	1973-2008	0.92	0.92
		Northern China	Southern China
Lu	1996-2010	0.78	0.87
EDGAR	1973-2008	0.91	0.88

3

1 Table 2. List of countries included to calculate regional SO₂ emission from the country-level
 2 emission data (countries with most parts inside the defined region) of S. J. Smith et al.
 3 (2011a).

Region	Countries
Eastern US	United States
Eastern Europe	Albania, Belarus, Bosnia & Herzegovina, Bulgaria, Czech, Croatia, Greece, Hungary, Latvia, Lithuania, Moldova, Poland, Romania, Serbia & Montenegro, Slovakia, Slovenia, Turkey, Ukraine
Western Europe	Austria, Belgium, Denmark, France, Germany, Ireland, Italy, Netherland, Portugal, Spain, Switzerland, United Kingdom

1 Figure 1. An example of change point detection and determination based on the time series of
2 50th (red) and 75th (black) percentiles of monthly $1/Vis$. Automatically detected change
3 points are represented by vertical lines. Text in the inset lists the dates of automatically
4 detected points. In this example, 5 significant change points are identified, in which February
5 1988 is determined as the separation point for further analysis, while other reported breaks are
6 considered as false detections.

7 Figure 2. Distribution of Integrated Surface Database (ISD) stations before (left) and after
8 (right) data screening. Colors indicate the number of years with available visibility data for
9 (upper) 1929-2013 and (lower) 1995-2013.

10 Figure 3. Spatial distribution of: (top left) average of the collocated b_{ext} of IMPROVE
11 stations, (top right) Pearson correlation coefficients between collocated pairs of monthly ISD
12 $1/Vis$ and IMPROVE b_{ext} , (bottom left) slope of monthly b_{ext} against monthly $1/Vis$ after
13 linear fitting through the origin point using the reduced major-axis linear regression (Ayers,
14 2001), and (bottom right) Pearson correlation coefficients between collocated pairs of
15 monthly ISD $1/Vis$ and EMEP $PM_{2.5}$.

16 Figure 4. Spatial distribution of relative trends in $1/Vis$ (top row), IMPROVE b_{ext} (middle
17 row), and IMPROVE b_{sp} (bottom row) over the US for 1989-2013. Larger colored points with
18 black outline indicate trends with at least 95% significance, smaller colored points with black
19 outline represent trends with 90%-95% significance, and colored points without outline
20 indicate insignificant trends. Stations with cross and circle symbols are collocated between
21 the ISD and IMPROVE networks over 1989-1996 for composite time series analysis in Fig. 6.

22 Figure 5. Spatial distribution of relative trends in $1/Vis$ and $PM_{2.5}$ over Europe for 2006-2013.
23 Larger colored points with black outline indicate trends with at least 95% significance,
24 smaller colored points with black outline represent trends with 90%-95% significance, and
25 colored points without outline indicate insignificant trends. Stations with cross and circle
26 symbols are collocated between the ISD and EMEP networks for composite time series
27 analysis in Fig. 6.

28 Figure 6. Composite time series and trends of (top) $1/Vis$ and b_{ext} for collocated ISD and
29 IMPROVE stations (Fig. 4) over 1989-1996 and (bottom) $1/Vis$ and $PM_{2.5}$ for collocated ISD
30 and EMEP stations (Fig. 5) over 2006-2013. Only stations with significant trends of >90%
31 confidence are collocated. The long ticks on the horizontal axis indicate the January of the

1 year. Data gaps represent months with less than 75% of the total grids. Error bars show the
2 25th and 75th percentile of all monthly values of collocated stations.

3 Figure 7. Spatial distribution of relative trends in $1/V_{is}$ over the US for 1945-1988. Larger
4 colored points with black outline indicate trends with at least 95% significance, smaller
5 colored points with black outline represent trends with 90%-95% significance, and colored
6 points without outline indicate insignificant trends. The red rectangle defines the eastern US
7 region for composite time series analysis in Fig. 8.

8 Figure 8. Composite time series of $1/V_{is}$ and SO_2 emission over the eastern US region. The
9 long ticks on the horizontal axis indicate January of the year, where all annual values are
10 plotted. Light green dots represent the average monthly $1/V_{is}$ of all qualified stations (error
11 bars showing the 25th and 75th percentile) in the defined region. Red dots show the number
12 of grid cells for averaging, and data gaps indicate months with less than 75% of the total grids
13 for each period. Blue lines and text represent the $1/V_{is}$ trends calculated using the monthly
14 anomalies for each period. Trends in parentheses are the 95% confidence intervals. Black
15 lines are the annual $1/V_{is}$ averaged from at least 8 monthly values. SO_2 emissions for the
16 entire US from S. J. Smith et al. (2011a) are in orange. Purple indicates EDGAR SO_2
17 emissions for the entire US (dashed) and for the defined region (solid) in Fig. 7.

18 Figure 9. Spatial distribution of relative trends in $1/V_{is}$ over Europe for 1973-2005. Larger
19 colored points with black outline indicate trends with at least 95% significance, smaller
20 colored points with black outline represent trends with 90%-95% significance, and colored
21 points without outline indicate insignificant trends. Red rectangles define the Eastern and
22 Western Europe regions for composite time series analysis in Fig. 10.

23 Figure 10. Regional time series analysis of $1/V_{is}$ and SO_2 emission over Western and Eastern
24 Europe. The long ticks on the horizontal axis indicate January of the year, where all annual
25 values are plotted. Light green dots represent the average monthly $1/V_{is}$ of all qualified
26 stations (error bars showing the 25th and 75th percentile) in the defined region. Red dots
27 show the number of grid cells for averaging, and data gaps indicate months with less than
28 75% of the total grids for each period. Blue lines and text represent the $1/V_{is}$ trends calculated
29 using the monthly anomalies for each period. Trends in parentheses are the 95% confidence
30 intervals. Black lines are the annual $1/V_{is}$ averaged from at least 8 monthly values. The Smith
31 SO_2 emissions in orange are the total emission of all countries listed in Table 2 for each

1 region. The EDGAR SO₂ emissions in purple are summed from all pixels inside the defined
2 region (Fig. 9).

3 Figure 11. Spatial distribution of relative trends in 1/Vis over Eastern Asia for 1973-2013.
4 Larger colored points with black outline indicate trends with at least 95% significance,
5 smaller colored points with black outline represent trends with 90%-95% significance, and
6 colored points without outline indicate insignificant trends. Red rectangles define the northern
7 and southern China regions for composite time series analysis in Fig. 12.

8 Figure 12. Regional time series analysis of 1/Vis and SO₂ emission over southern and
9 northern China. The long ticks on the horizontal axis indicate January of the year, where all
10 annual values are plotted. Light green dots represent the average monthly 1/Vis of all
11 qualified stations (error bars showing the 25th and 75th percentile) in the defined region. Red
12 dots show the number of grid cells for averaging, and data gaps indicate months with less than
13 75% of the total grids for each period. Blue lines and text represent the 1/Vis trends calculated
14 using the monthly anomalies for each period. Trends in parentheses are the 95% confidence
15 intervals. Black lines are the annual 1/Vis averaged from at least 8 monthly values. The SO₂
16 emission in Lu et al. (2011) in orange and the EDGAR SO₂ emission in purple are summed
17 from all pixels inside the defined region (Fig. 11).

18 Figure A1. Threshold visibility of ISD stations over the US, Europe and Eastern Asia in 1990,
19 1995 and 2000.

20 Figure A2. Scatter plot of monthly b_{sp} (measured by nephelometers) and b_{ext} (estimated from
21 aerosol speciation data) from all IMPROVE stations with b_{sp} measurements for 56 IMPROVE
22 sites over 1993-2013. The intercept of $\sim 12 \text{ Mm}^{-1}$ corresponds to Reyleigh scattering.

23 Figure A3. SO₂ emission for several major countries. Data are from S. J. Smith et al. (2011a).
24 The top left and top right panels include major countries of Western and Eastern Europe,
25 respectively. Vertical lines represent division years of the study periods that roughly indicate
26 transition points of emission trend.

27 Figure A4. Spatial distribution of relative trends in 1/Vis over the US for 1929-1944. Larger
28 colored points with black outline indicate trends with at least 95% significance, smaller
29 colored points with black outline represent trends with 90%-95% significance, and colored
30 points without outline indicate insignificant trends.

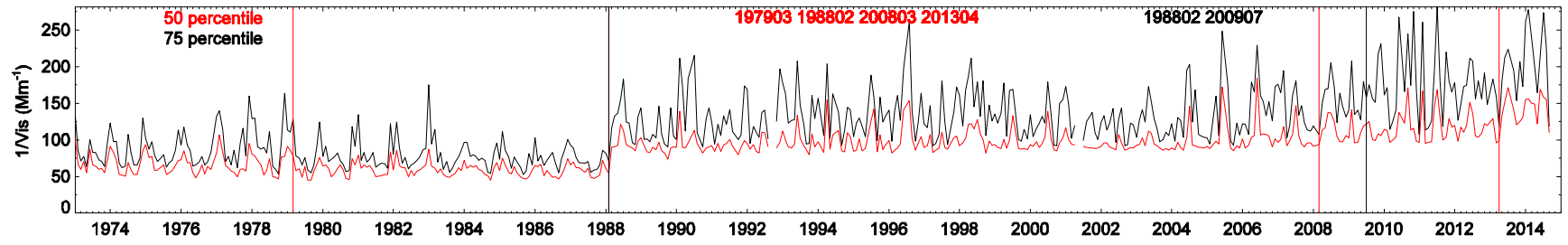


Figure 1.

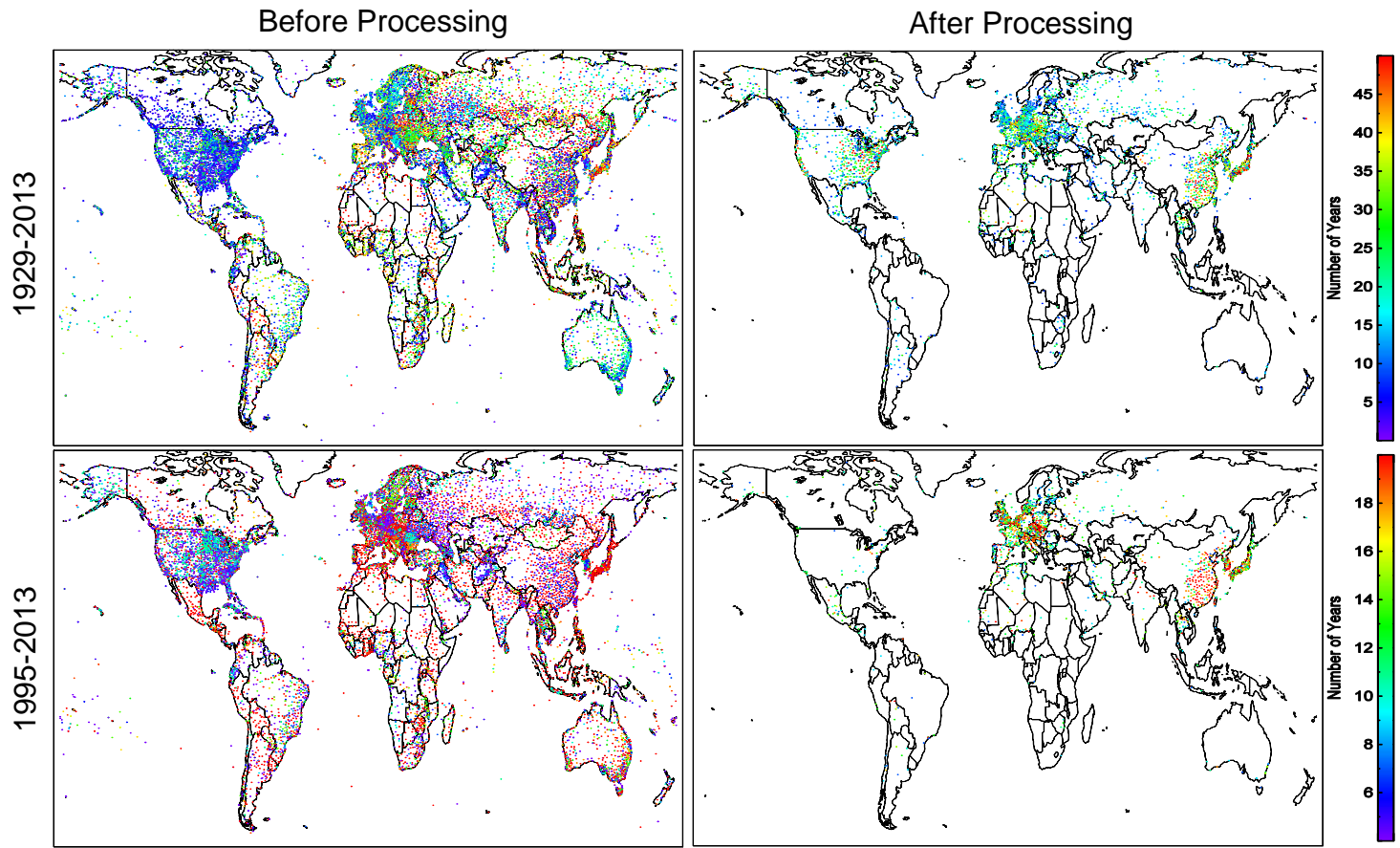


Figure 2.

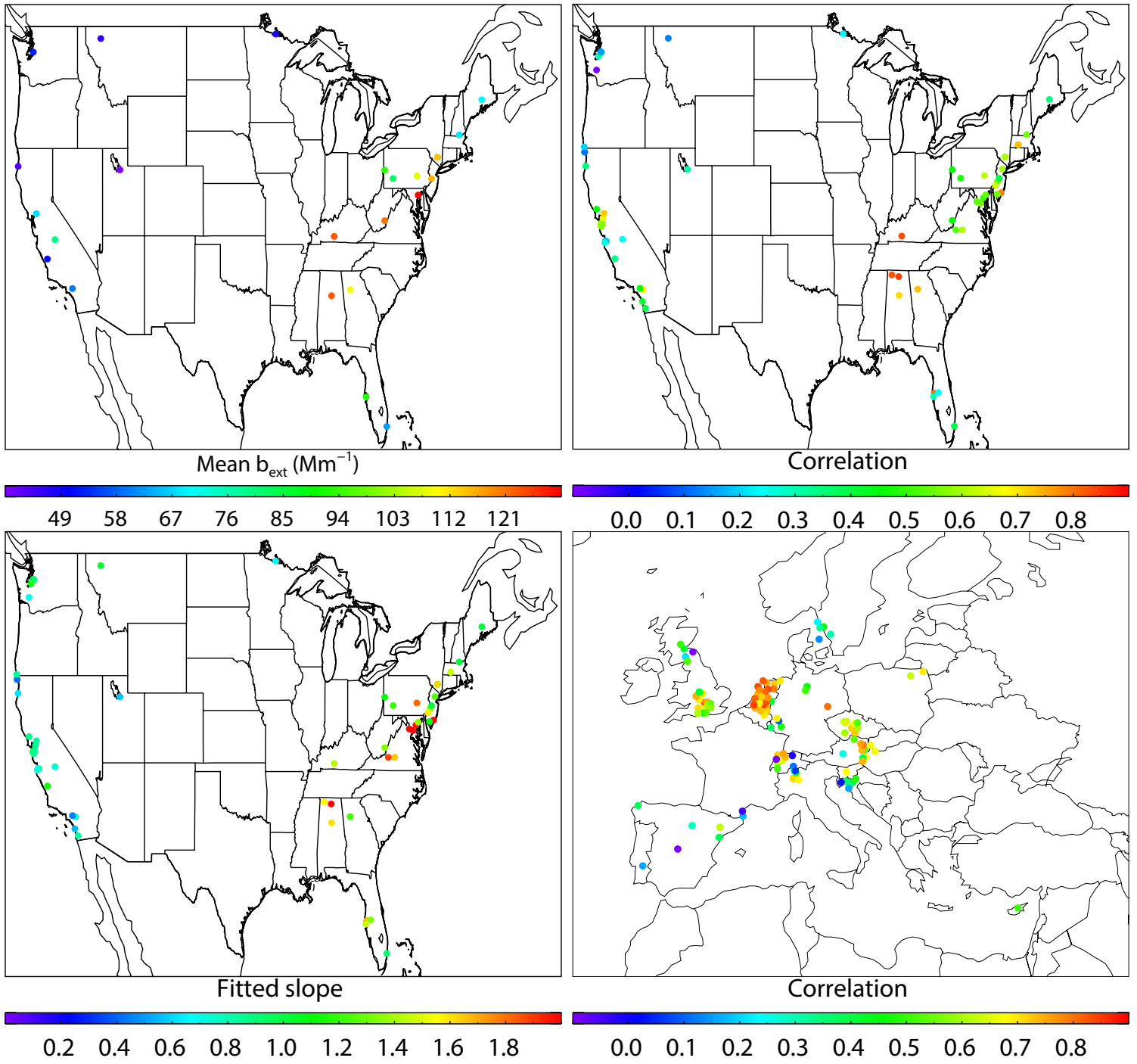
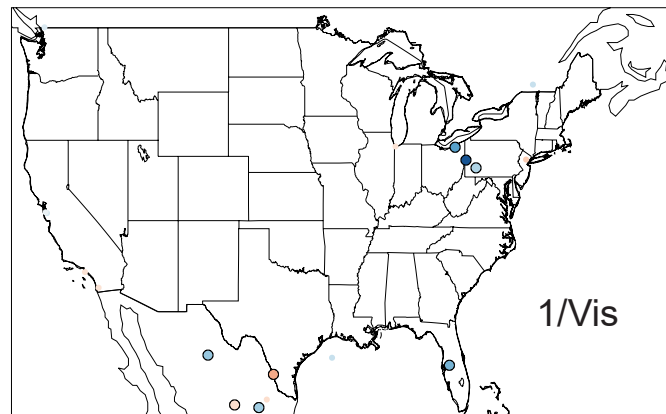
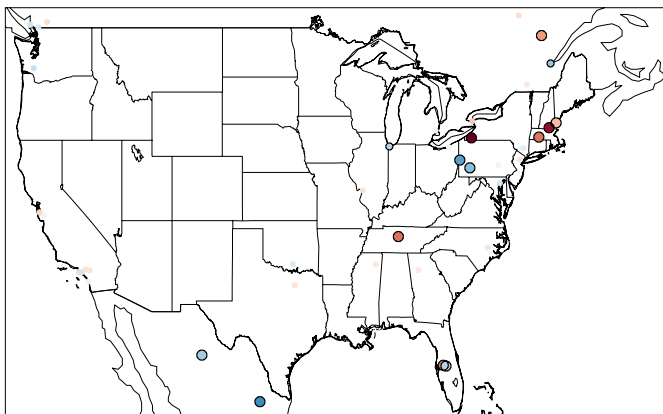
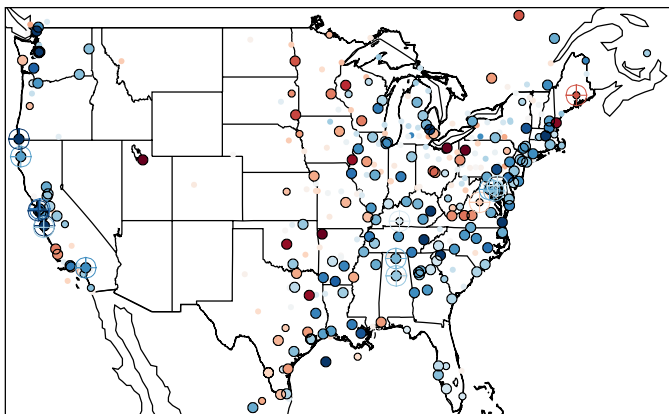


Figure 3.

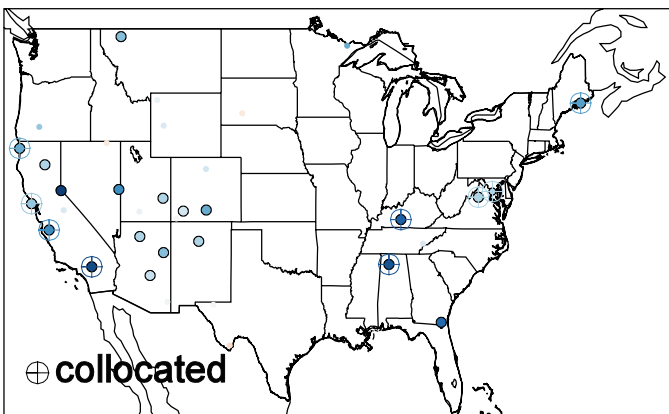
1989-1996

1997-2005

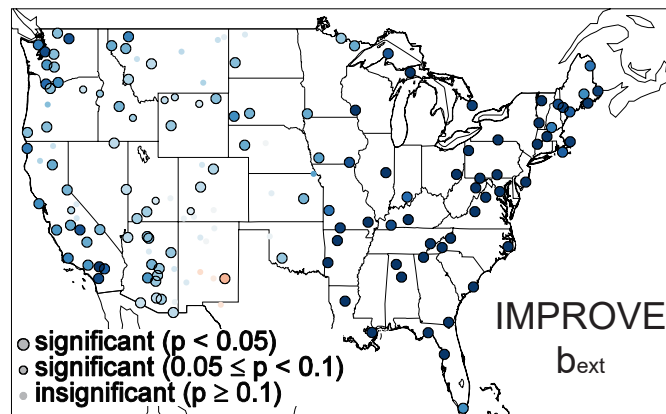
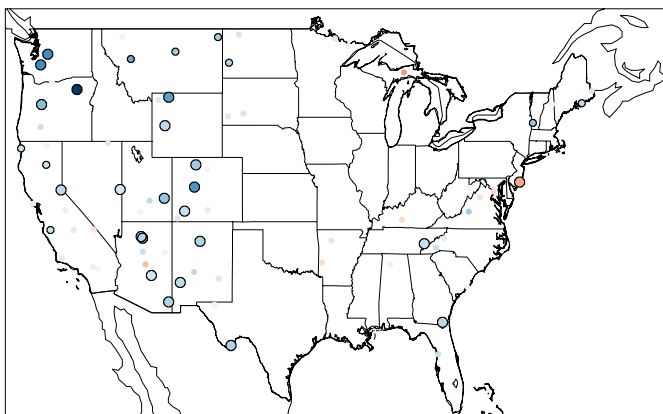
2006-2013



1/Vis

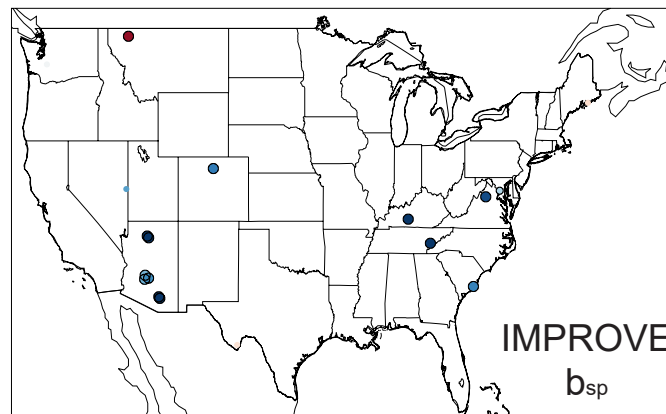
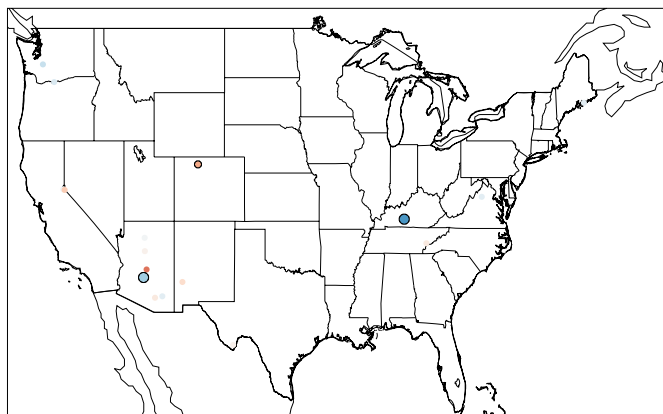


⊕ collocated



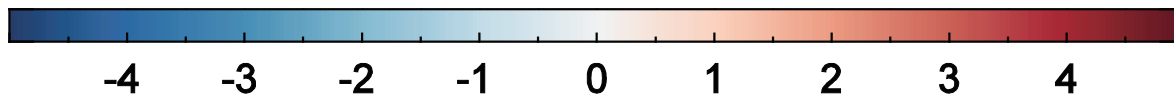
○ significant ($p < 0.05$)
○ significant ($0.05 \leq p < 0.1$)
○ insignificant ($p \geq 0.1$)

IMPROVE
b_{ext}



IMPROVE
b_{sp}

trend (%/year)



-4 -3 -2 -1 0 1 2 3 4

Figure 4.

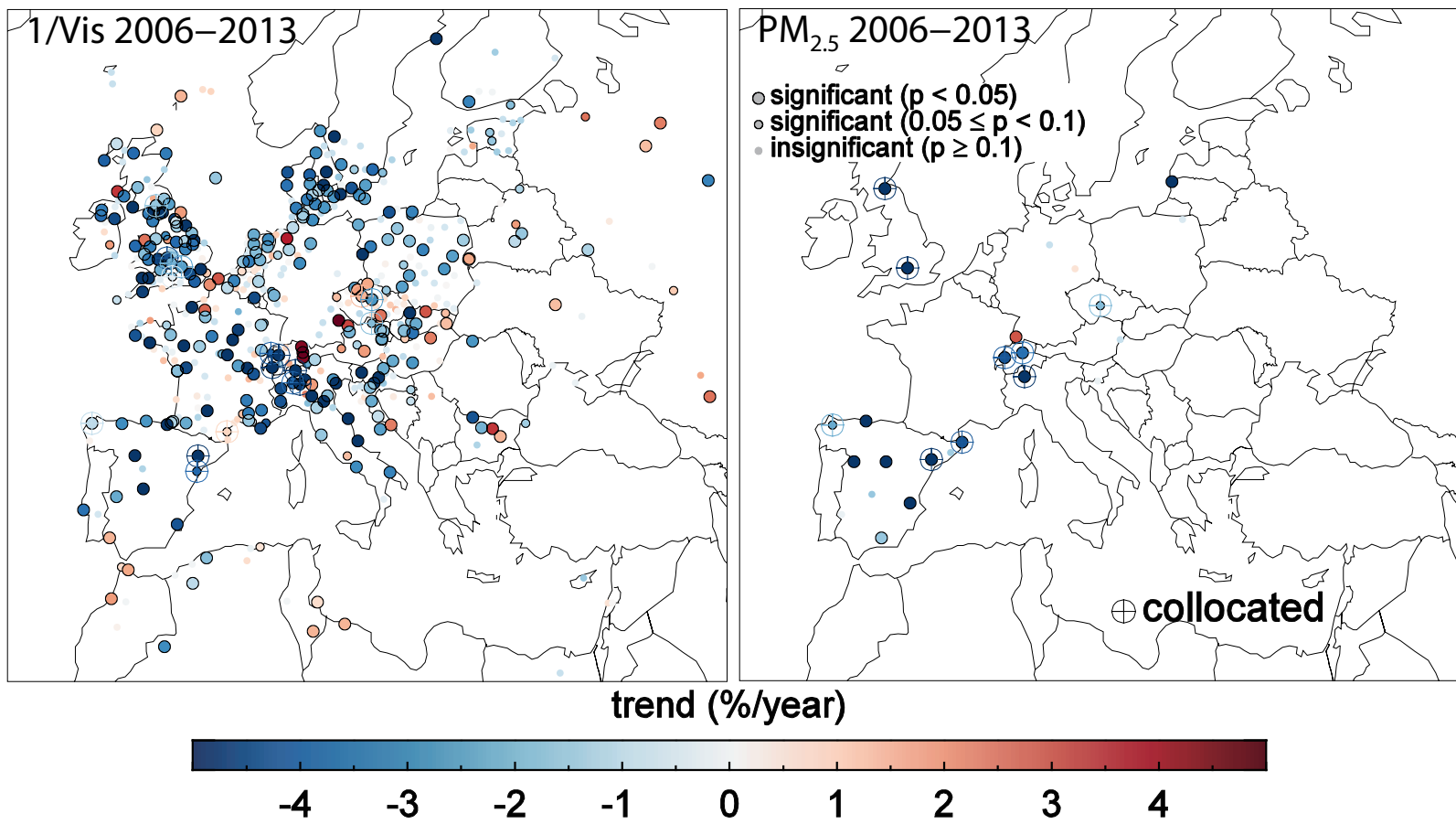


Figure 5.

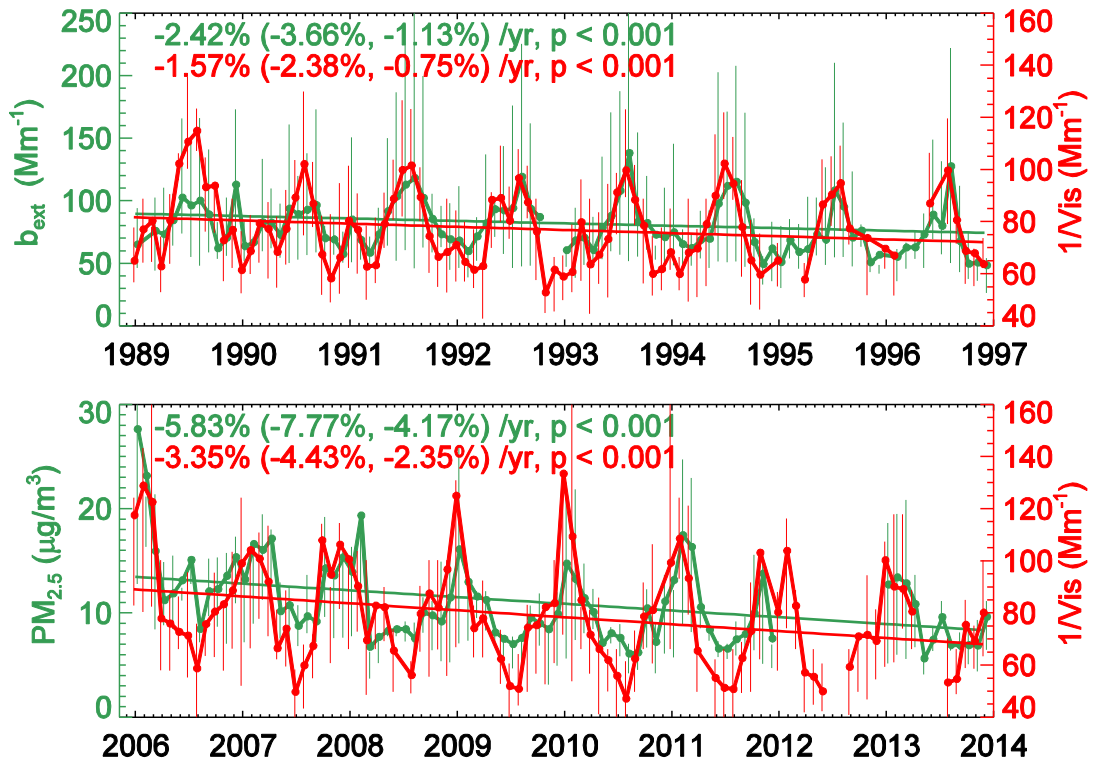


Figure 6.

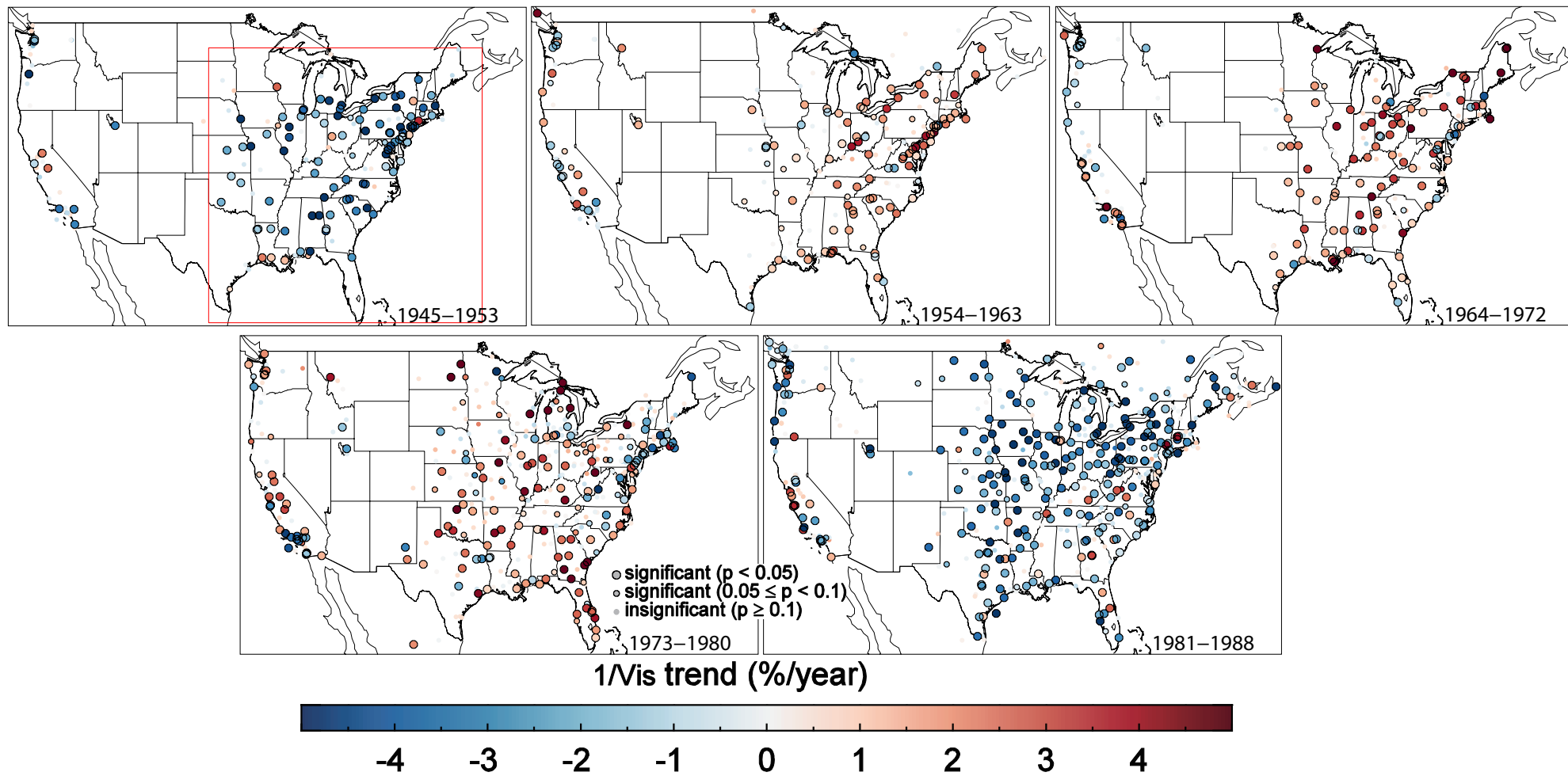


Figure 7.

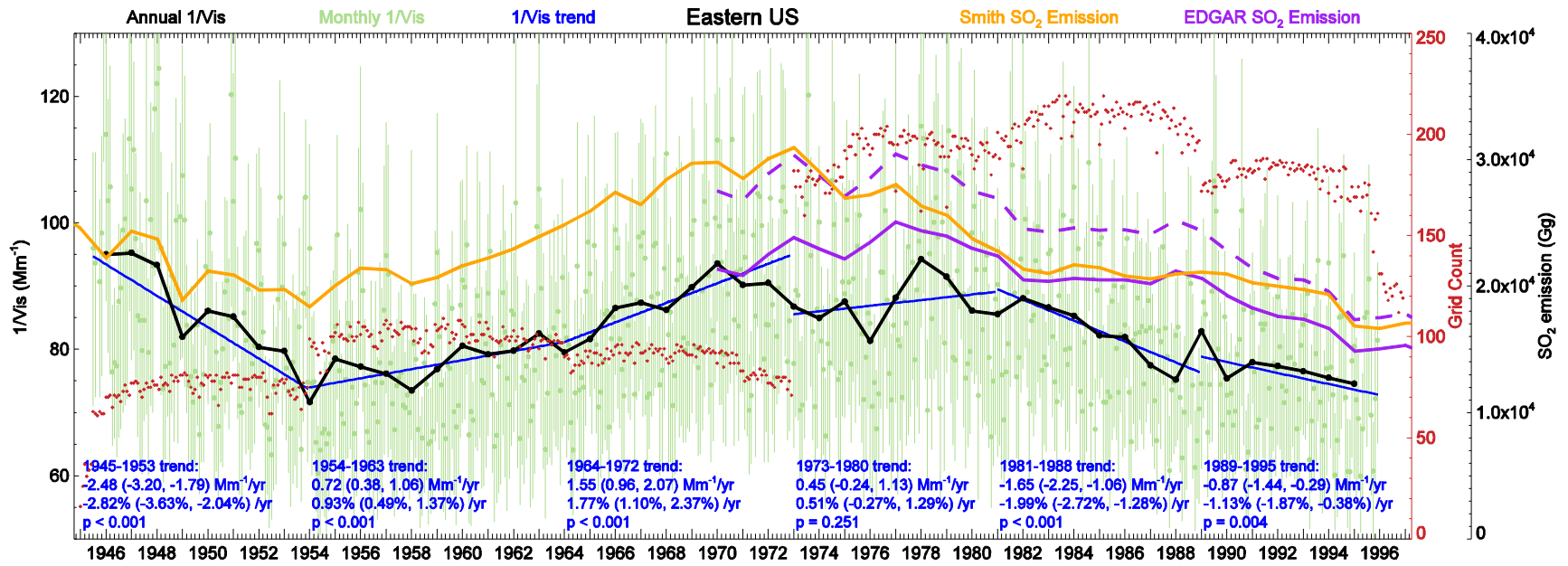


Figure 8.

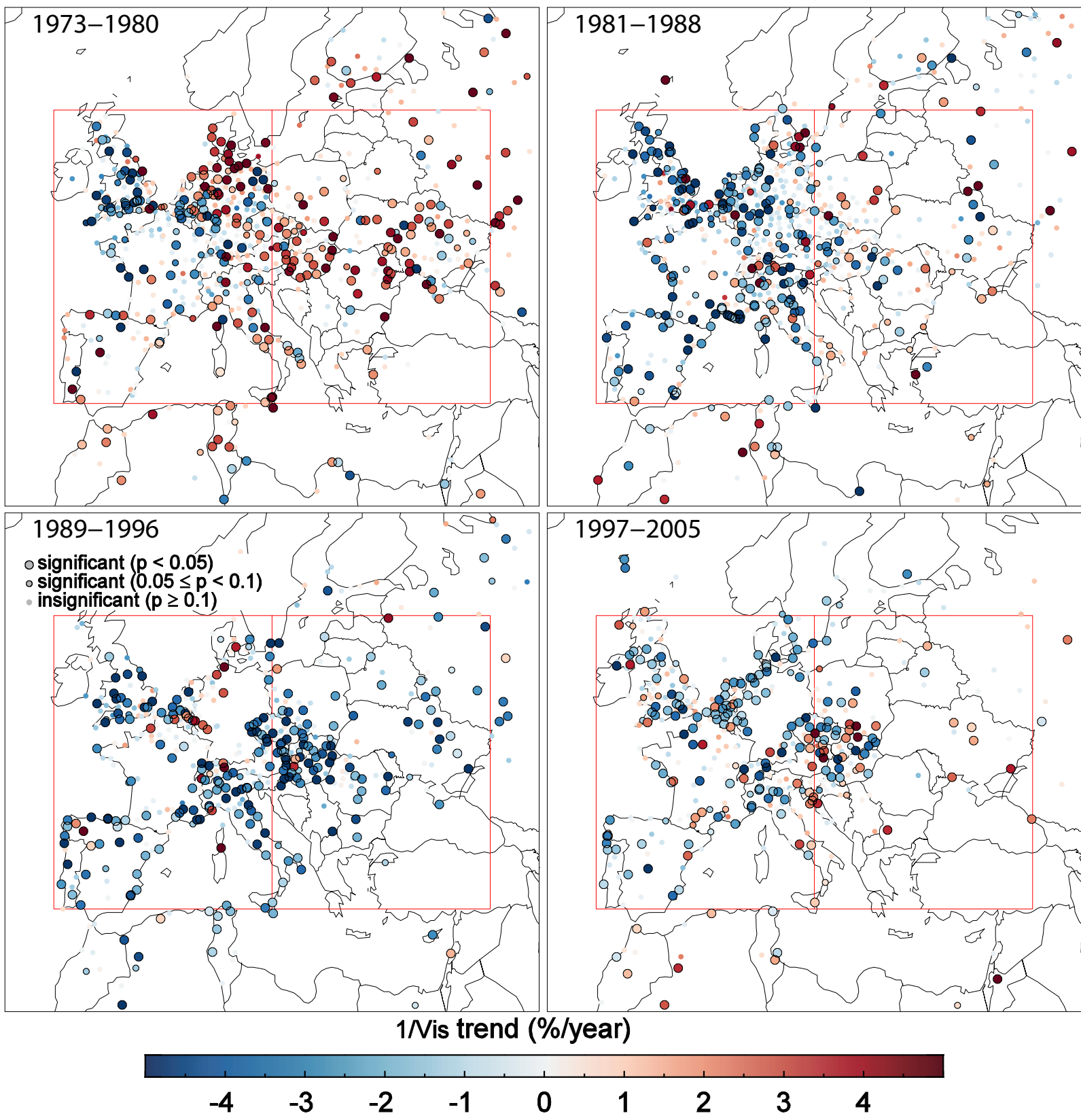


Figure 9.

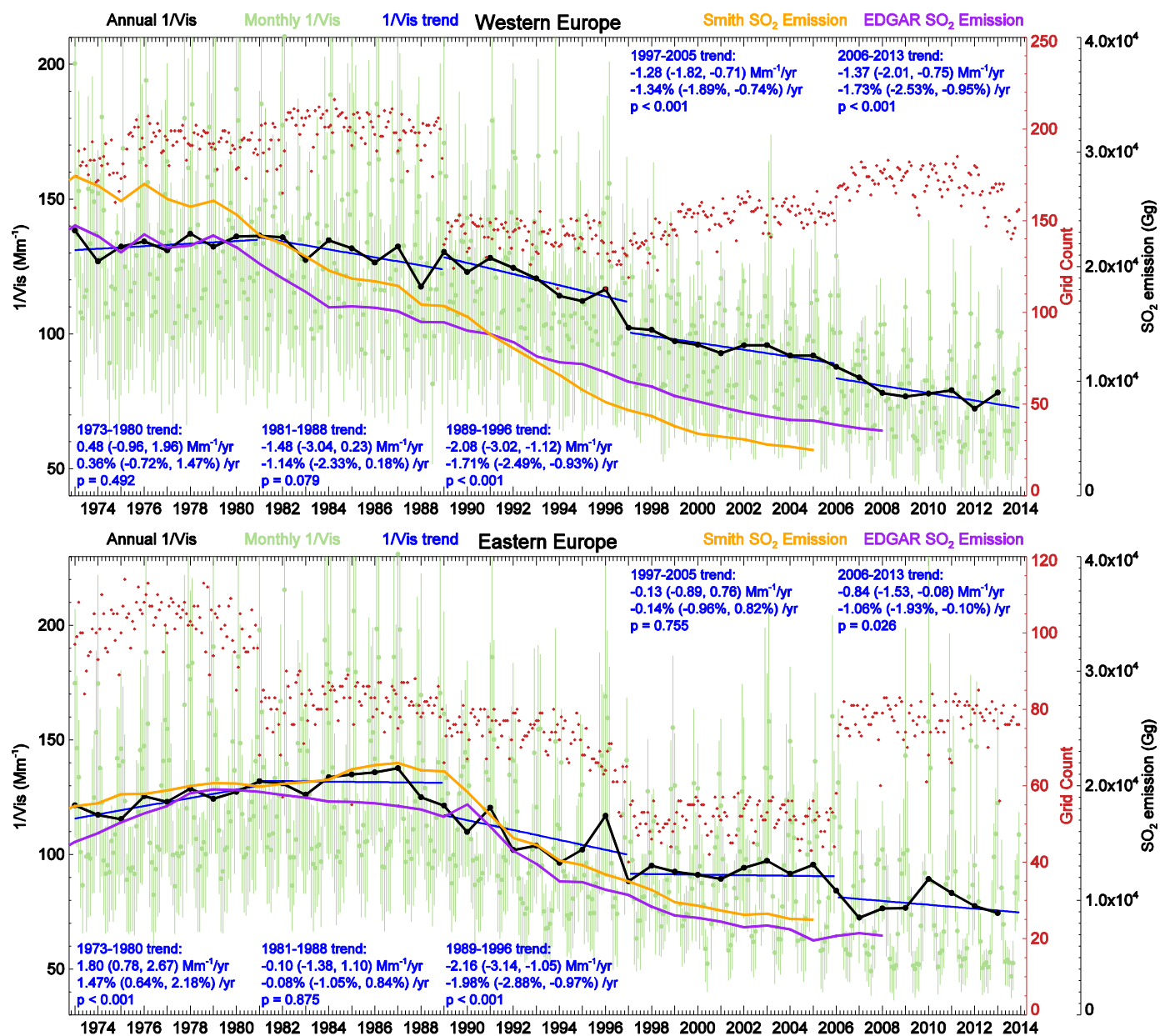


Figure 10.

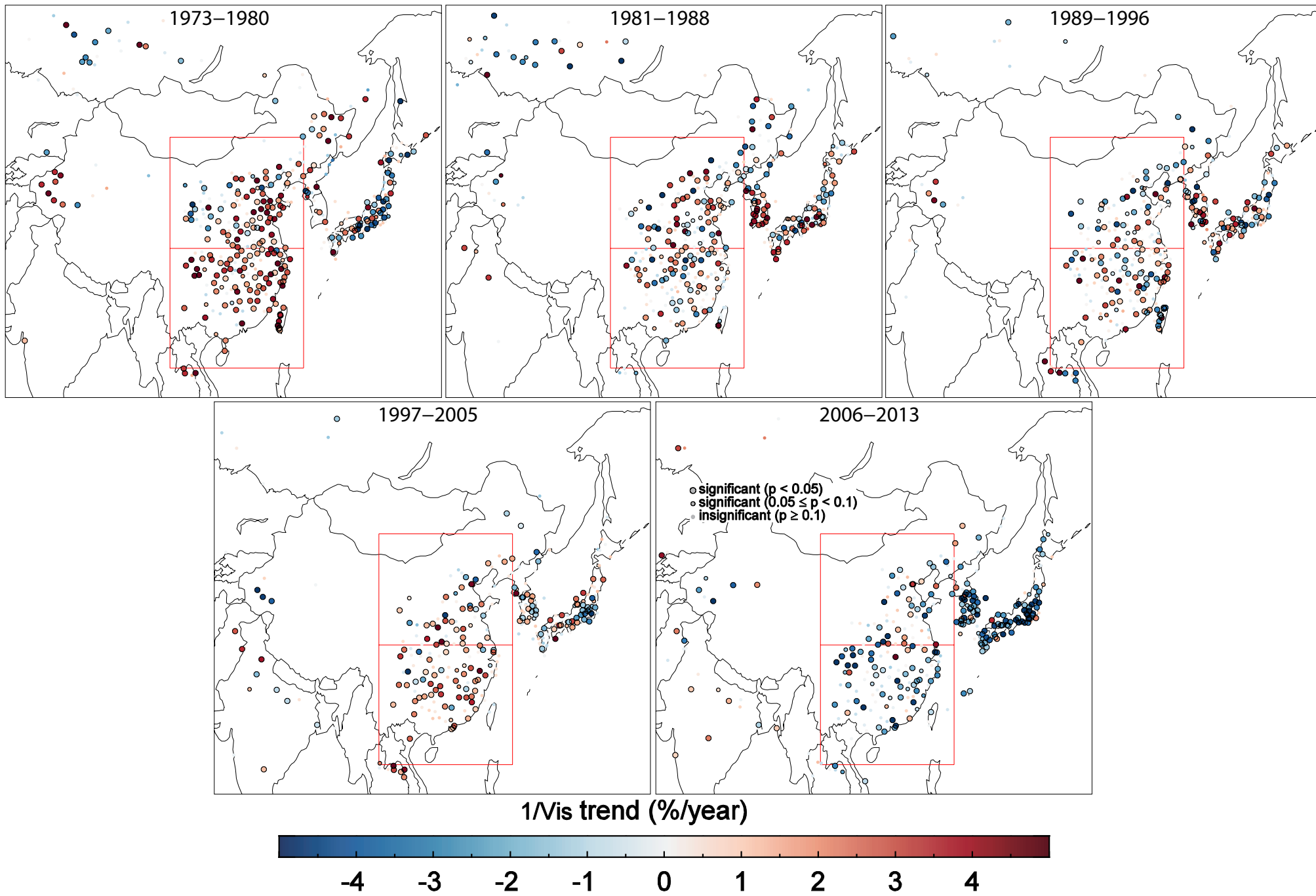


Figure 11.

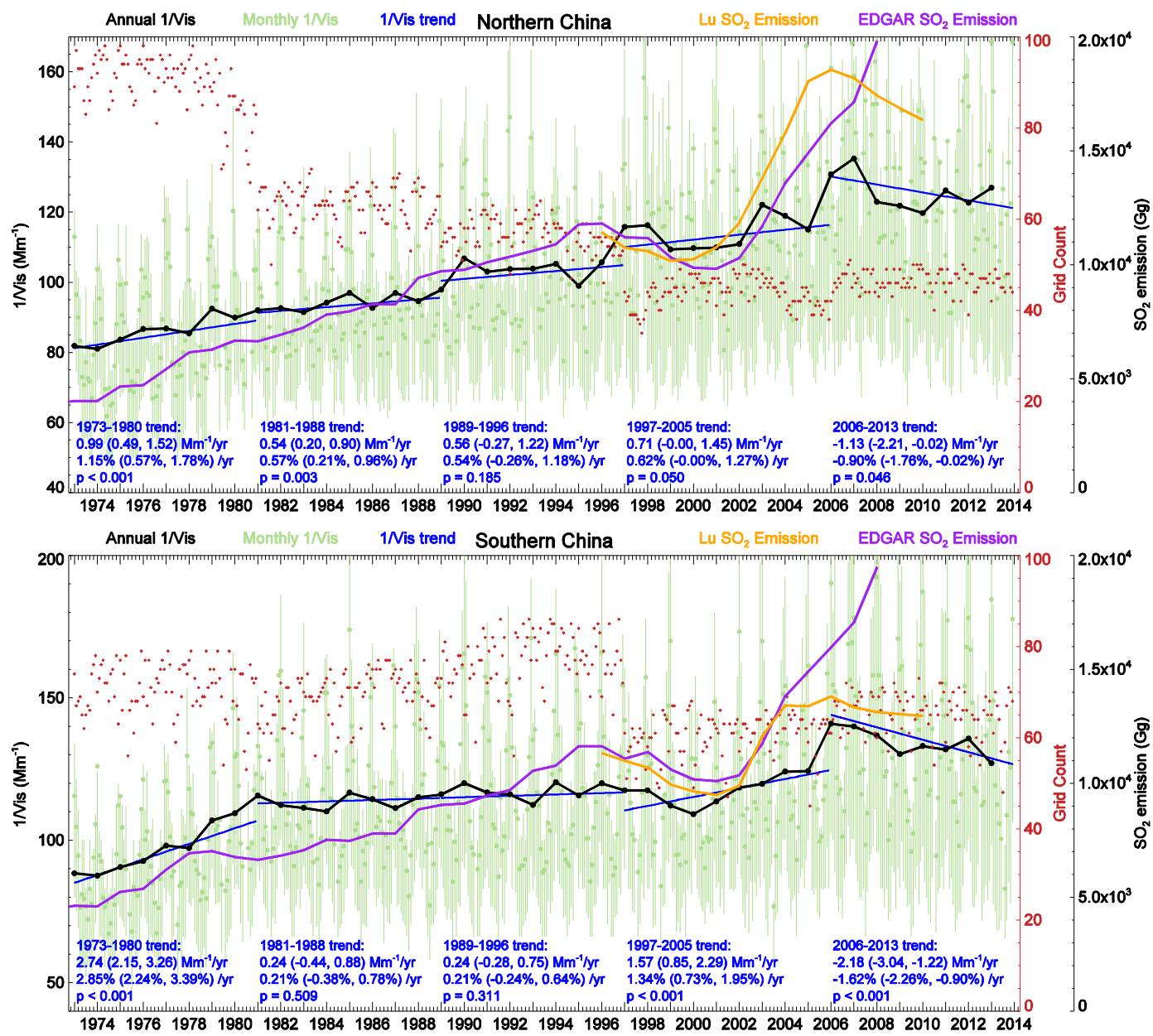


Figure 12.

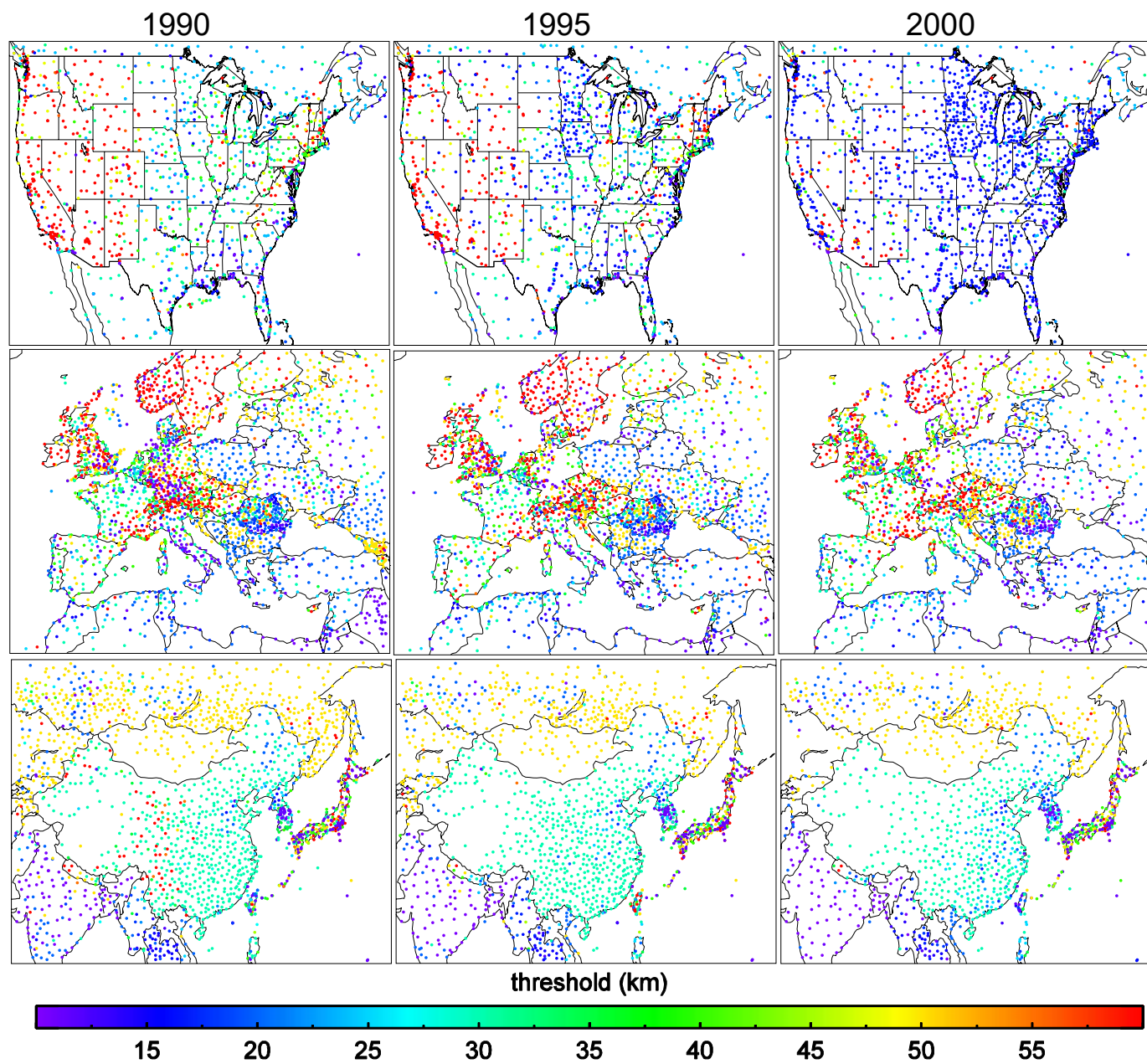


Figure A1.

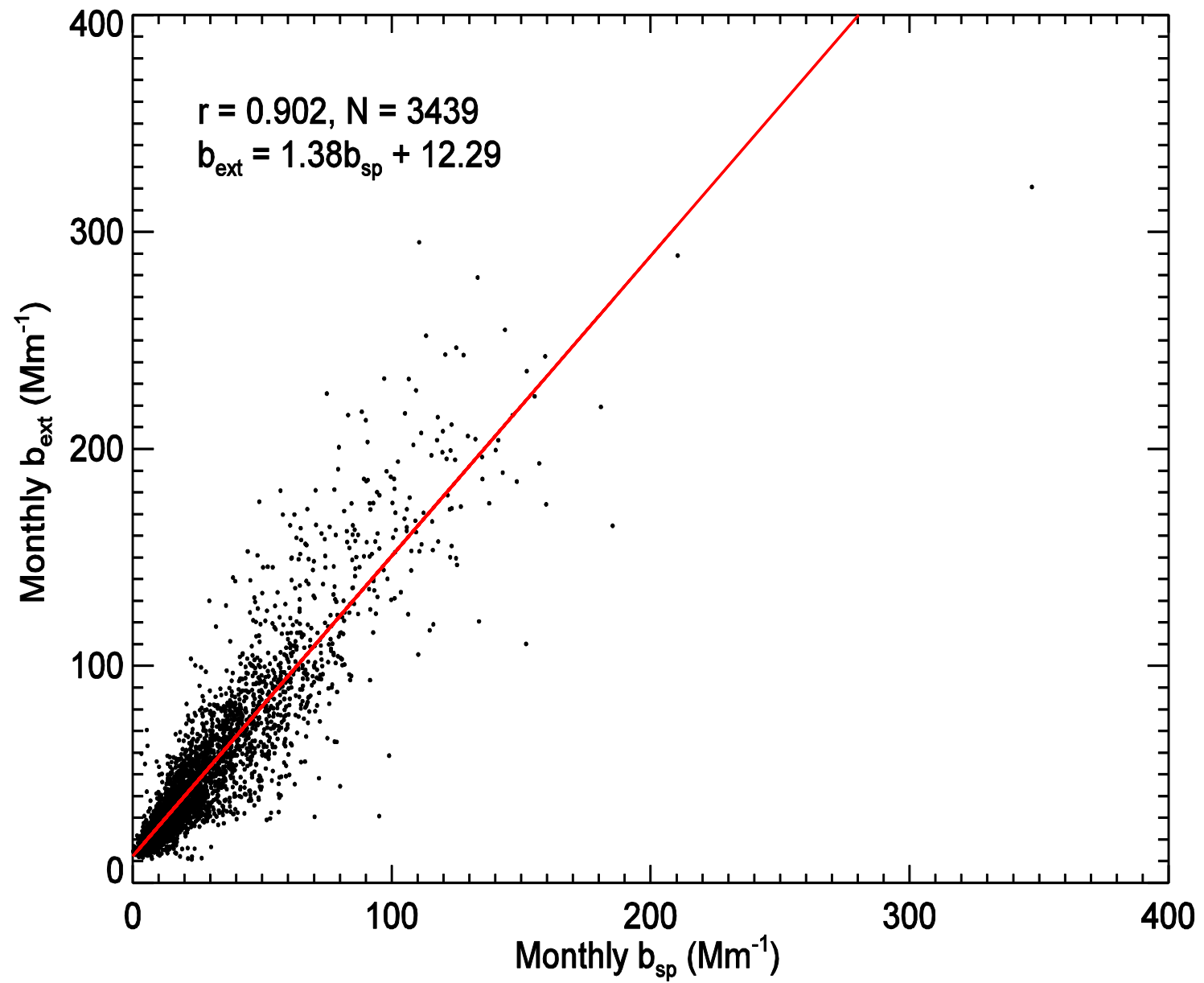


Figure A2.

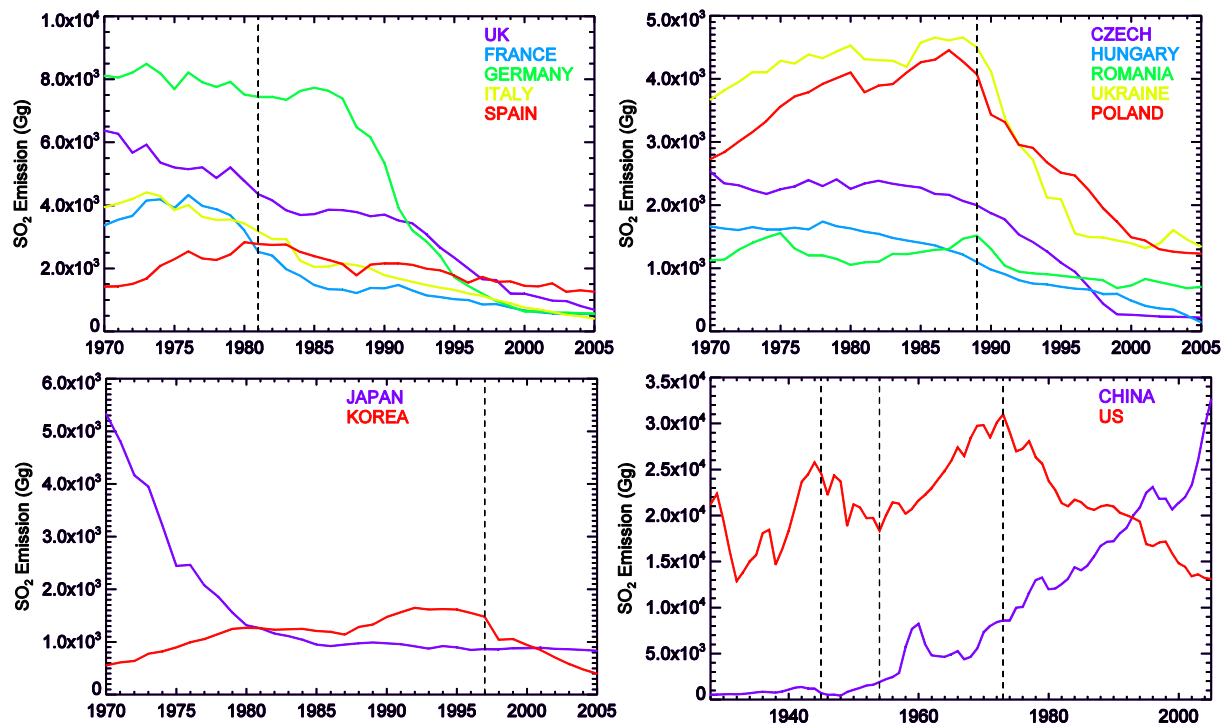


Figure A3.

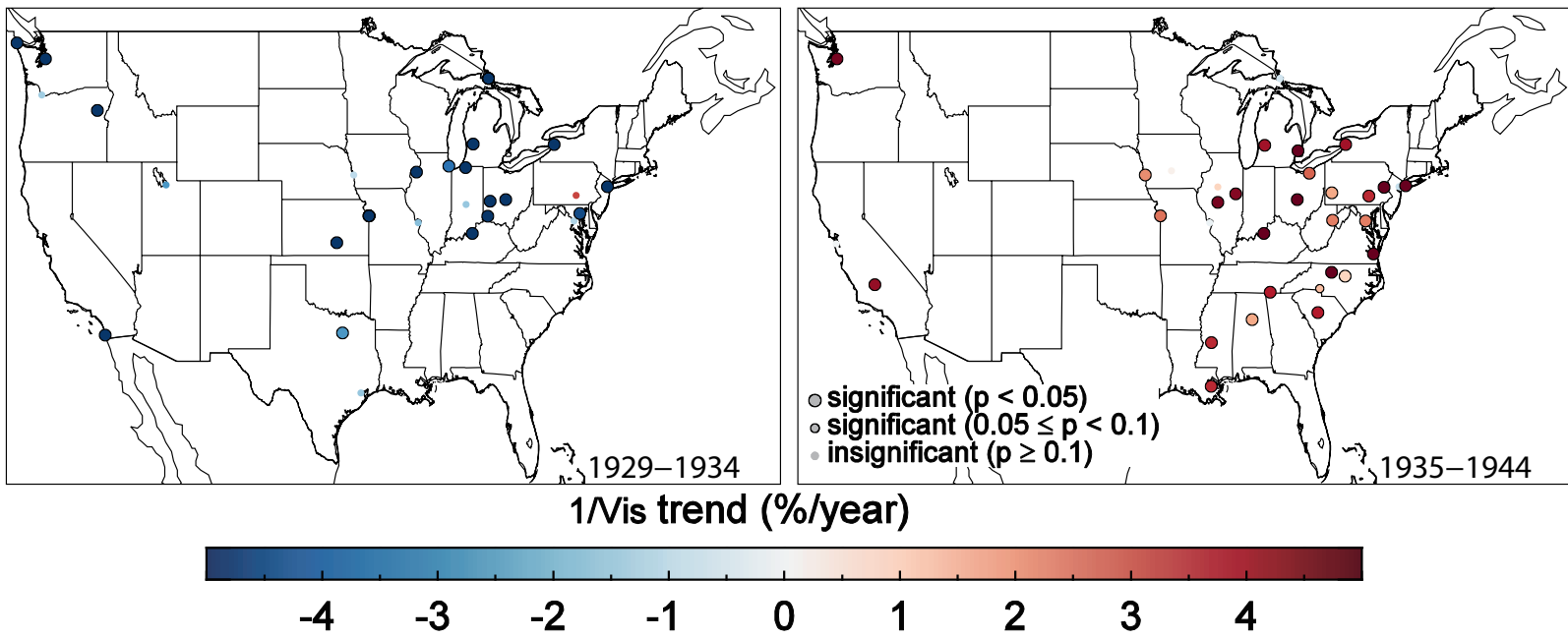


Figure A4.